HHS Public Access

Author manuscript

Dysphagia. Author manuscript; available in PMC 2021 August 06.

Published in final edited form as:

Dysphagia. 2020 June ; 35(3): 419–437. doi:10.1007/s00455-019-10045-6.

A Surgical Mouse Model for Advancing Laryngeal Nerve Regeneration Strategies

Alexis Mok[#1], **Jakob Allen**[#2], **Megan M. Haney**[3], **Ian Deninger**[4], **Brayton Ballenger**[4], **Victoria Caywood**[4], **Kate L. Osman**[4], **Bradford Zitsch**[2], **Bridget L. Hopewell**[4], **Aaron Thiessen**[4], **Marlena Szewczyk**[2], **Daniel Ohlhausen**[4], **Christopher I. Newberry**[2], **Emily Leary**[5], **Teresa E. Lever**[4,6]

[1]Department of Communication Science and Disorders, University of Missouri School of Health Professions, Columbia, MO, USA

[2]Department of Medicine, University of Missouri School of Medicine, Columbia, MO, USA

[3]Department of Veterinary Pathobiology, University of Missouri College of Veterinary Medicine, Columbia, MO, USA

[4]Department of Otolaryngology – Head & Neck Surgery, University of Missouri School of Medicine, Columbia, MO, USA

[5]Department of Orthopedic Surgery, University of Missouri School of Medicine, Columbia, MO, USA

[6]One Hospital Dr. MA314, Columbia, MO 65212, USA

[#] These authors contributed equally to this work.

Abstract

Iatrogenic recurrent laryngeal nerve (RLN) injury is a morbid complication of anterior neck surgical procedures. Existing treatments are predominantly symptomatic, ranging from behavioral therapy to a variety of surgical approaches. Though laryngeal reinnervation strategies often provide muscle tone to the paralyzed vocal fold (VF), which may improve outcomes, there is no clinical intervention that reliably restores true physiologic VF movement. Moreover, existing interventions neglect the full cascade of molecular events that affect the entire neuromuscular pathway after RLN injury, including the intrinsic laryngeal muscles, synaptic connections within the central nervous system, and laryngeal nerve anastomoses. Systematic investigations of this pathway are essential to develop better RLN regenerative strategies. Our aim was to develop a translational mouse model for this purpose, which will permit longitudinal investigations of the pathophysiology of iatrogenic RLN injury and potential therapeutic interventions. C57BL/6J mice were divided into four surgical transection groups (unilateral RLN, $n = 10$; bilateral RLN, $n = 2$;

[✉]Teresa E. Lever, levert@health.missouri.edu.

Conflict of interest The authors declare that they have no other potential conflicts of interest.

Research Involving Human Participants and/or Animals No human participants were included in this study, only animals. All applicable international, national, and/or institutional guidelines for the care and use of animals were followed. All procedures performed in studies involving animals were in accordance with the ethical standards of the institution or practice at which the studies were conducted.

unilateral SLN, $n = 10$; bilateral SLN, $n = 10$) and a sham surgical group ($n = 10$). Miniaturized transoral laryngoscopy was used to assess VF mobility over time, and swallowing was assessed using serial videofluoroscopy. Histological assays were conducted 3 months post-surgery for anatomical investigation of the larynx and laryngeal nerves. Eight additional mice underwent unilateral RLN crush injury, half of which received intraoperative vagal nerve stimulation (iVNS). These 8 mice underwent weekly transoral laryngoscopy to investigate VF recovery patterns. Unilateral RLN injury resulted in chronic VF immobility but only acute dysphagia. Bilateral RLN injury caused intraoperative asphyxiation and death. VF mobility was unaffected by SLN transection (unilateral or bilateral), and dysphagia (transient) was evident only after bilateral SLN transection. The sham surgery group retained normal VF mobility and swallow function. Mice that underwent RLN crush injury and iVNS treatment demonstrated accelerated and improved VF recovery. We successfully developed a mouse model of iatrogenic RLN injury with impaired VF mobility and swallowing function that can serve as a clinically relevant platform to develop translational neuroregenerative strategies for RLN injury.

Keywords

Deglutition; Deglutition disorders; Laryngeal nerve; Regeneration; Dysphagia; Animal model; Electrical stimulation

Introduction

Iatrogenic recurrent laryngeal nerve (RLN) injury, a complication of anterior neck surgical procedures, results in ipsilateral vocal fold (VF) immobility and associated dysphagia, dysphonia, and dyspnea [1–3]. Although the RLN may spontaneously regenerate after injury, recovery may take several months to years, and full return of normal function rarely occurs [2, 4, 5]. Poor outcomes are largely attributed to pathological reinnervation of the intrinsic laryngeal muscles, either by preferential reinnervation of laryngeal adductors by regenerating RLN fibers or by collateral reinnervation by the superior laryngeal nerve (SLN) [2, 6, 7]. While pathological reinnervation may mitigate laryngeal muscle atrophy, VF movement typically remains ineffective and unsynchronized [6, 8, 9]. Older individuals are particularly at risk for worse outcomes, as aged peripheral nerves have reduced regenerative capacity [10–12]. This biological deficiency is especially concerning for the increasingly aging population undergoing anterior neck procedures [13, 14].

Existing treatments for RLN injury are predominantly symptomatic, ranging from behavioral therapy to a variety of surgical approaches. Though laryngeal reinnervation strategies often provide muscle tone to the paralyzed VF, which may improve functional outcomes, there is no clinical intervention that reliably restores true physiologic VF movement [15–19]. Moreover, existing interventions neglect the full cascade of molecular events that affect the entire neuromuscular pathway after RLN injury, including the intrinsic laryngeal muscles, synaptic connections within the central nervous system, and laryngeal nerve anastomoses. Systematic investigations of this pathway are essential to develop better RLN regenerative strategies. Animal models such as pigs [20–25], dogs [26], cats [27], rats [28, 29], and rabbits [15] provide suitable platforms for this purpose. Rats, in particular, are

at the forefront of an emerging treatment for nerve regeneration—electrical stimulation applied proximal to the nerve injury site. This approach has shown promising effects after facial nerve [30, 31] and RLN [29] injury. However, these studies have predominantly focused on infant or young adult rats whose developing nervous systems bear little resemblance to mature humans. Moreover, no animal study of RLN injury has integrated basic science techniques with the clinical gold standard combination of endoscopy and videofluoroscopy for clinicopathological investigation of the aerodigestive tract.

The goal of this study was to develop a *mouse* surgical model of iatrogenic RLN injury to accelerate scientific discovery. We chose the C57BL/6J mouse because it is an established translational model for investigations of swallowing [32] and laryngeal biology [33]. The short life-span of the mouse permits high-throughput, longitudinal investigations in aged populations more representative of anterior neck surgical patients. However, its small size (Fig. 1) has been prohibitive to the development of directly translatable functional outcome measures for correlation with histological findings [34]. Here, we have overcome this challenge by using our “miniaturized” endoscopic [35] and fluoroscopic [32, 36] imaging methodology to develop a translational mouse model of iatrogenic RLN injury.

Our first endeavor was to ensure the fidelity of the laryngeal innervation pattern and functional outcomes between humans and mice. We focused on transection (neurotmesis) injuries because they are most experimentally replicable [5], and included the RLN and SLN because of the growing evidence of dual innervation of the intrinsic laryngeal muscles [37, 38]. We hypothesized that like humans, RLN transection in mice would cause chronic impairment of VF mobility and dysphagia, whereas SLN transection would result in subtle, transient changes in VF mobility and swallowing function. Furthermore, we expected more severe symptoms after bilateral injury. Finally, we adapted our model to include a more prevalent crush (axonotmesis) injury [5], and conducted a feasibility study of intraoperative vagal nerve stimulation (iVNS) as a novel RLN regenerative strategy. In doing so, we expanded upon a recent study in young adult rats in which RLN stimulation accelerated the recovery of VF mobility after RLN crush injury [29]. However, rather than stimulating the RLN, we chose the cervical vagus nerve as a more clinically relevant treatment site to simultaneously target all potentially injured RLN branches and promote widespread regeneration. Moreover, we tested this strategy in aged mice to better correspond to the average age of anterior neck surgical patients, thus highlighting our translational intent.

Materials and Methods

Animals

Fifty adult C57BL/6 (also known as B6) mice of either sex were included in this study, which was approved by our Institutional Animal Care and Use Committee. The majority of these mice ($n = 42$) were used to develop our surgical model of iatrogenic laryngeal nerve injury (i.e., transection), and the remaining ($n = 8$) were allowed to age for further model refinement (i.e., RLN crush injury and exploratory regenerative treatment). All mice were offspring from our C57BL/6 J colony established by mating sibling pairs purchased at 6 weeks of age from The Jackson Laboratory (Bar Harbor, ME). Over a 2-year period, offspring between 3 and 12 months of age were randomly assigned to several surgical

cohorts, with transection injury groups completed before beginning the crush injury component of this investigation.

Mice were group housed (2–4 animals per cage, based on sex and litter) in a standard 12:12 light/dark cycle facility with controlled temperature and humidity conditions. Free access to water and standard rodent food pellets was provided, except during the experimental procedures described below. An enhanced enrichment protocol (e.g., running wheel and chewable treats) was used for all cages to minimize aggression and the need for single housing in our aging B6 colony. Daily monitoring by veterinary and research staff ensured that all mice remained healthy throughout the study.

Surgical Procedures

General Surgical Approach—All 50 mice underwent microsurgery using a midline ventral neck approach, closely following our previously established methods [39]. After a 4–6-h food restriction, mice were anesthetized with a single subcutaneous injection of ketamine-xylazine (90/11.25 mg/kg), followed by scheduled maintenance doses of ketamine (half the original dose) every 10–20 min as needed to maintain a surgical plane of anesthesia (i.e., absence of pedal withdrawal and eye blink reflexes). Eyes were lubricated (Lacrilube®, Allergan, Inc.; Irvine, CA) to prevent drying. The ventral neck was shaved and prepared aseptically for surgery. Next, the head was stabilized in ear bars, with the mouse positioned in dorsal recumbency on a custom surgical platform beneath a surgical microscope (M125; Leica Microsystems, Inc., Buffalo Grove, IL). Core body temperature was maintained at 37 ± 0.2 °C using a homeothermic heating system (DC Temperature Controller; FHC, Bowdoin, ME). Mice spontaneously breathed room air during the entire surgical procedure, except during iVNS treatment, when supplemental oxygen was provided (described below).

Immediately prior to the surgical neck incision, laryngoscopy (described below) was performed according to our published protocol [35] to establish baseline VF function. Next, an approximate 2-cm midline skin incision was made from the suprasternal notch to the intersection of the anterior digastric muscles near the mandibular symphysis, using a micro-scalpel and micro-scissors. The large salivary glands were gently retracted from midline with micro-forceps and secured with a pediatric ophthalmic retractor for unobstructed visualization of the surgical field (Fig. 2a). The target laryngeal nerve was visualized within the fascia along the lateral aspect of the larynx (SLN) or trachea (RLN). After careful isolation using micro-forceps, laryngeal nerve injury was performed according to experimental group assignment (transection versus crush injury, described below).

Immediately following surgical manipulation, laryngoscopy was repeated to assess the effect on VF mobility (described below). Next, soft tissue structures were approximated medially, and the neck incision was closed with 6–0 monocryl suture material (Ethicon™, Johnson & Johnson Company; New Brunswick, NJ) and surgical glue (Tissumend II, Veterinary Products Laboratories; Phoenix, AZ). Post-surgical analgesics (buprenorphine, 0.05 mg/kg; banamine, 2.2 mg/kg) and saline (0.2 mL) were administered subcutaneously prior to transferring mice to a recovery cage warmed to 37 °C on a water-circulating heating pad (Model #TP700, Stryker Medical, Portage, MI). Mice were returned to their home cage when fully ambulatory, typically within 1 h after surgery. For 72 h post-surgery, pain

management (buprenorphine, 0.05 mg/kg) was provided every 8–12 h, and the home cage was kept warm by placing it half way on a 37 °C water-circulating heating pad (Stryker) to prevent anesthesia-related hypothermia. Post-operative monitoring was conducted daily by research staff for 1 week, and then daily health monitoring by animal care staff continued throughout the remainder of the study.

Laryngeal Nerve Transection Injury—Mice (n = 42) were randomly allocated to one of five surgical groups: unilateral RLN transection (n = 10), bilateral RLN transection (n = 2, due to anticipated mortality from mechanical asphyxiation), unilateral SLN transection (n = 10), bilateral SLN transection (n = 10), and sham surgery (n = 10). *For RLN transection*, the strap muscles overlying the trachea were retracted from midline between the 4th and 6th tracheal rings to visualize the RLN running alongside the inferior thyroid artery (Fig. 2b). *For SLN transection*, the SLN was readily identified within the superficial fascia on the lateral aspect of the larynx, traveling alongside the superior laryngeal artery (Fig. 2c). *For the unilateral nerve injury groups*, only the right side was included because it was the most ergonomic for our custom surgical set-up and workflow. The target laryngeal nerve (either SLN or RLN, unilateral or bilateral) was gently isolated from the surrounding fascia and blood vessels with micro-forceps. The nerve was then transected with micro-scissors and a 1–2-mm section was removed to prevent spontaneous re-attachment of the proximal and distal nerve stumps during recovery. The transection location was always proximal (i.e., closer to the central nervous system) to any visible branches from the main nerve trunk. Sham surgery mice underwent all aspects of the surgical procedure, except the laryngeal nerves were visualized within the fascia and isolated, but not transected. For all surgical groups, laryngoscopy was repeated at the end of the procedure to assess the effect of surgical manipulation on VF mobility.

Immediately prior to transection of the SLN, a confirmatory step of brief electrical stimulation (described below) was added to assure that we had indeed identified the correct nerve. Previous work in our lab [39] and others [40] has shown that 40 Hz stimulation of the SLN (main trunk) in mice reliably evokes swallowing. In contrast, RLN stimulation parameters to evoke swallowing in mice have not yet been established, and our preliminary work (unpublished) has shown that 40 Hz stimulation of the RLN in mice does *not* reliably evoke swallowing. Therefore, correct targeting of the RLN was confirmed by endoscopic visualization of ipsilateral VF immobility immediately after surgical transection.

For SLN stimulation, we used custom, bipolar hook electrodes (FHC, Bowdoin, ME) made of platinum iridium, with a 300 μm tip diameter, spaced 800 μm apart. The electrodes were positioned near the SLN using a manual micromanipulator (model U-30CF; Narishige, Co, LPD, Setagaya-Ku, Tokyo, Japan), and the SLN was gently draped over the electrodes using micro-hooks. Electrical stimulation was delivered continuously for a single 20-s train using our previously published parameters for evoking SLN-stimulated swallowing in mice: 40 Hz, biphasic 0.5 ms square wave pulses, with a 0.1-ms interphase delay, delivered at 800 μA [39]. Stimulation was delivered using a constant current stimulus isolator (model 1101; ADInstruments, Colorado Springs, CO) coupled to an A/D converter (PowerLab 8/30, ADInstruments), with both devices controlled by LabChart software (ADInstruments). Current flow was directed *toward* the brain by positioning the anode electrode distal to the

cathode electrode on each nerve, with directionality verified using a current probe (model P6042; Tektronic, Beaverton, OR) and voltage meter (True RMS MultiMeter; Extech Intruments, Waltham, MA). The stimulus shape and intensity were continually verified using a digital oscilloscope (model TDS 2024B; Tektronix) connected to the stimulus isolator. Swallowing events were identified by endoscopic visualization of tongue base retraction in conjunction with observable laryngeal elevation within the surgical site; both events were simultaneously video recorded at 30 frames per second (fps) via the endoscope camera and surgical microscope camera. If no swallowing events were observed, visible exudate around the SLN was absorbed using paper points (#501; Henry Schein, Inc., Melville, NY), the nerve was repositioned on the bipolar electrode to prevent any contact with the surrounding tissues, and then a 2nd 20-s stimulus train was delivered. For the bilateral SLN transection group, this stimulation approach was performed separately for each side.

RLN Crush Injury and iVNS Treatment—For this feasibility study, we included 8 aged mice (over 12 months old) from our B6 colony to expand the utility and translatability of our surgical model. Rather than a transection (neurotmesis) injury, all 8 mice underwent a right-sided RLN crush (axonotmesis) injury. To do this, the RLN was carefully isolated from the fascia and inferior thyroid artery between the 4th and 6th tracheal rings using micro-forceps. Next, a micro-hook was used to place the RLN perpendicularly across smooth jaw hemostatic forceps (1 mm tip diameter, 13007–12; FST, Foster City, CA), which were then closed to the second locking position for 30 s [41].

Laryngoscopy was repeated after RLN crush injury to assess the immediate effect on VF mobility. Mice were then randomly allocated to iVNS treatment ($n = 4$) or control ($n = 4$) groups. For the iVNS treatment group, the right cervical vagus nerve was isolated from the carotid sheath and placed on our previously described hook electrodes for continuous electrical stimulation at 20 Hz, as has been used for previous cranial nerve regeneration studies in rats [29–31, 42]. For the control group, the vagus nerve was neither isolated nor placed on electrodes after the RLN crush injury.

During iVNS treatment, current flow was directed *toward* the brain by positioning the anode electrode distal to the cathode electrode on the vagus nerve, with directionality verified as described above. This approach ensured that iVNS-evoked action potentials traveled *toward* the central nervous system to stimulate the cell bodies of the injured axons, which is essential for triggering upregulation of neurotrophic factors, their receptors, and growth associated proteins that accelerate regeneration at the distal nerve injury site [43, 44]. We used our standard stimulus waveform parameters (biphasic 0.5 ms square wave pulses, with a 0.1-ms interphase delay) to deliver 20-s stimulus trains continuously for up to 60 min, depending on respiratory tolerance (described below). Stimulus intensity was increased from 0.2 to 0.8 mA in 0.1 mA steps to quickly (within 1–2 min) identify the highest subthreshold intensity level that did not evoke swallowing or cause agonal/labored breathing. This subthreshold stimulus level was then used for iVNS treatment, with the waveform morphology (shape and intensity) continually verified via oscilloscope, as described above.

During the additional surgical time required for the iVNS-treated mice, supplemental oxygen was provided via a nose cone at 1 L/min, and respiratory rate was monitored every

10 min throughout the treatment duration. If agonal/labored breathing developed during iVNS treatment, the stimulus intensity level was lowered in 0.1 mA steps to quickly (within 1–2 min) identify the level at which breathing stabilized; this new subthreshold level was used for the remainder of the iVNS treatment. If respiratory status was not stabilized by lowering the stimulus intensity, iVNS treatment was immediately stopped to prevent ensuing morbidity or mortality.

Functional Measures

Laryngoscopy and VFSS were conducted at baseline (pre-surgery) and several post-surgical time points to assess VF mobility and swallowing function, respectively, during a 3-month recovery period, as described below. Post-surgical VFSS was always conducted 3–5 days before laryngoscopy to avoid confounding effects of anesthesia (required for laryngoscopy) on VFSS outcomes.

VF Mobility—To assess VF mobility, laryngoscopy was performed according to our established protocol [35], with mice under surgical plane of anesthesia while spontaneously breathing room air (Fig. 3). Laryngoscopy was performed twice during the surgical procedure—immediately before surgical incision (to record baseline bilateral VF movement during spontaneous breathing) and again following surgical manipulation (to determine the immediate effect on VF mobility). Additionally, laryngoscopy was performed at multiple post-surgical time points with mice under brief (< 15 min), surgical-level sedation. Mice allocated to the transection protocol underwent post-operative laryngoscopy at 1 week and 3 months post-surgery to assess acute versus chronic effects, respectively, on VF mobility. Mice allocated to the RLN crush/iVNS protocol underwent laryngoscopy more frequently (i.e., weekly) to better characterize the pattern of spontaneous functional recovery versus treatment efficacy.

Our laryngoscopy protocol entailed securing anesthetized mice in ear bars in dorsal recumbency on our custom surgical platform. Next, a sialendoscope (R11573A; Karl Storz) with a custom laryngoscope was inserted transorally and advanced via a custom micromanipulator to visualize the larynx on a Storz Tele Pack X monitor (Karl Storz Endoskope, Tuttlingen, Germany). The endoscope was slowly advanced until the bilateral VFs filled the entire field of view, and VF movement was video recorded at 30 fps for approximately 1 min during spontaneous breathing. Videos (MP4 files) were viewed frame-by-frame by two independent reviewers (authors TEL and BZ or MMH) using video editing software (Pinnacle Studio 14, Pinnacle Systems, Inc., Mountain View, CA), and VF mobility was scored using a subjective rating scale: 2 = normal movement, 1 = reduced movement, and 0 = no movement [28, 45]. Reviewer discrepancies were resolved by group consensus with the principal investigator (TEL).

Swallow Function—Mice allocated to the transection protocol underwent VFSS testing according to our standard, freely behaving (unanesthetized) protocol [32, 36] (Fig. 4) at 3 time points: baseline (i.e., approximately 1 week prior to surgery) as well as 1 week and 3 months post-surgery to assess acute versus chronic effects, respectively. Mice allocated to

the RLN crush/iVNS treatment protocol were not subjected to VFSS testing in order to minimize resources used for this feasibility study.

Beginning 2 weeks prior to baseline VFSS testing, mice underwent a behavioral conditioning program to assure familiarity and acceptance of the contrast solution and test environment. At each VFSS time point, mice were fluid restricted overnight for 14–16 h and provided additional chewable enrichment (e.g., nut and seed mix) to motivate voluntary drinking during VFSS testing the following morning. During testing, mice were individually enclosed in a custom VFSS test chamber secured to a custom, remote-controlled lift table within our miniaturized fluoroscope (Glenbrook Technologies, Randolph, NJ). Each mouse was then exposed to approximately 2–3 min of low-dose radiation (~ 30 kV and 0.2 mA) for fluoroscopic examination of swallowing in the lateral plane while freely drinking a species-specific oral contrast agent recipe: Omnipaque (350 mg iodine per mL; GE Healthcare, Inc., Princeton, NJ) diluted to a 25% solution with deionized water and 3% chocolate syrup. The contrast solution was administered through a custom delivery system into a custom bowl positioned immediately above the test chamber floor. To minimize radiation exposure, the fluoroscope was activated only when mice were drinking from the bowl, which was identified by real-time viewing via a webcam (C920 HD Pro Webcam; Logitech International S.A., Lausanne, Switzerland) positioned above the VFSS test chamber. The oropharyngeal stage of swallowing was visualized first (Fig. 4c), followed by remote-controlled repositioning of the chamber to visualize the entire esophageal stage of swallowing in a single field of view (Fig. 4d). Fluoroscopic videos were captured at 30 fps during real-time viewing via computer monitor.

Videos (AVI files) were subsequently analyzed frame-by-frame by two independent reviewers (authors AM, VC, BB, DO, or ID) using video editing software (Pinnacle Studio 14) to quantify 6 swallow metrics established by our prior work [32, 36], as described in Table 1. We also quantified airway protection using the standardized 8-point Penetration-Aspiration Scale (PAS) that ranges from 1 (no penetration or aspiration) to 8 (silent aspiration) [46]. Reviewer discrepancies were resolved by group consensus with the principal investigator (TEL).

Histological Investigation

At the study end point (3 months post-surgery), mice were euthanized by transcardial perfusion with saline followed by 4% paraformaldehyde, and relevant tissues were collected for a variety of post-mortem assays. For gross anatomical mapping of the laryngeal nerves, a subset of samples ($n = 10$) were collected as whole head and thorax specimens for laryngeal nerve mapping using a modified Sihler staining protocol [47–50]. This lengthy (~ 6 months) 8-step technique, summarized in Table 2, rendered the entire specimen transparent while staining myelinated nerves a dark purple color. Stained specimens were examined under a dissection microscope (LM80; Leica) and carefully trimmed to remove soft tissue overlying the laryngeal nerves for improved visualization. Specimens were then placed on an X-ray light box beneath our surgical microscope (M125; Leica) for trans-illumination and digital imaging (Pixelink E421CU camera, Ottawa, Canada).

Another subset of samples ($n = 10$) was subjected to post-mortem dissection of the laryngeal nerves using our surgical (M125; Leica) and dissection (LM80; Leica) microscopes. A separate subset of samples ($n = 4$) underwent paraffin processing and embedding, sectioning by microtome (10 μm serial transverse sections), hematoxylin and eosin (H&E) staining, and light microscopy (DM4000, Leica), according to our standard protocols [39, 51]. Color processing of digital images via Photoshop CS5 (Adobe Systems, San Jose, CA) was used to enhance visualization of the anatomical regions of interest. For the remaining samples, the larynx and brain were collected to establish histological methods for subsequent use in a larger RLN crush injury/iVNS study.

Statistics

Basic summary statistics were calculated for each outcome measure of interest for each component of this investigation: laryngeal nerve transection injury (i.e., model development) and RLN crush/iVNS treatment (i.e., model refinement and therapeutic investigation). For the transection component, analysis was focused on three clinically relevant time points: (1) baseline (1 week prior to surgery), (2) 1 week post-surgery to capture acute functional changes in VF mobility and swallowing, and (3) at the end of the surgical recovery period (i.e., 3 months post-surgery; chronic recovery stage) to capture any functional improvement or progression of the surgical injury. One-way repeated measures ANOVAs and one-way ANOVAs were used to demonstrate differences in outcome measures across time and between surgical groups. Two-sample *t* tests were used to assess mean differences between a treated group and control. Some analyses used change scores rather than the original data values; change scores were calculated using the difference from each measure at each time point (acute or chronic recovery surgery), compared to baseline. If warranted, post hoc testing was performed using Tukey HSD. For the RLN crush/iVNS component, the small sample size ($n = 3$ per group) precluded rigorous statistical analyses. All statistics were calculated using SPSS v24 with a two-sided alpha of 0.05 to determine statistical significance.

Results

Six of the 50 mice (12%) included in this study died during the surgical procedure. Four of the 6 mice died unexpectedly from intraoperative respiratory distress: unilateral SLN transection ($n = 1$), unilateral RLN transection ($n = 1$), and RLN crush/iVNS ($n = 1$ in the 60-min treatment group, and $n = 1$ in the no treatment group). As expected, the 2 mice in the bilateral RLN transection group died from mechanical asphyxiation (i.e., VFs fixed in the median position) immediately after the 2nd RLN was transected. These 6 mice were excluded from statistical analysis, as no post-operative data were collected. Below, the results for the surviving 44 mice are summarized separately for the model development (i.e., transection injury, $n = 38$) and model refinement (i.e., RLN crush injury and iVNS treatment, $n = 6$) aims of this study.

Model Development: Laryngeal Nerve Transection Injury

Descriptive statistics for the 4 surgical groups are shown in Table 3. All 38 mice underwent functional testing of VF mobility (i.e., laryngoscopy) and swallowing (i.e., VFSS) as planned at each time point, with results described below.

VF Mobility—A total of 152 laryngoscopy videos (38 mice × 4 time points) were manually analyzed using a 3-point rating scale. Only RLN transection injury had an effect on VF mobility. Specifically, unilateral RLN transection resulted in immediate, ipsilateral VF immobility (i.e., fixation in the paramedian position; score = 0, Fig. 5) that persisted at the acute (1 week) and chronic (3 month) post-surgical time points. In contrast, SLN transection (unilateral or bilateral) had no effect on VF mobility, as the score remained unchanged (i.e., 2 = normal) across time points. Similarly, the sham surgery itself did not impair VF mobility. Change scores in VF mobility at the acute (1 week) versus chronic (3 month) post-surgical time points (compared to baseline function) are shown in Table 4. However, statistical analysis could not be performed because there was no variability in the data within treatment groups (i.e., standard deviation = 0).

Swallow Function—A total of 114 VFSS videos (38 mice × 3 time points) were manually analyzed to calculate 6 VFSS metrics as well as to assign a penetration-aspiration score for each mouse at each time point. Descriptive statistics are provided in Table 5. We first assessed the effect of the surgical injury itself (i.e., without laryngeal nerve transection) using a one-way repeated measures ANOVA. Results revealed that the mean value for each variable was not statistically different between time points, thus validating that the surgical procedure does not cause dysphagia.

Three VFSS metrics (swallow rate, lick–swallow ratio, and inter-swallow interval) were problematic for hypothesis testing because mean values for both SLN transection groups were statistically different from the RLN transection and sham surgical groups at baseline, but not at post-surgical time points. Therefore, we conducted separate one-way ANOVAs at each time point (rather than using change scores which utilizes baseline values) at the 1-week and 3-month post-surgery time points to facilitate model development. No statistically significant differences were identified between surgical groups for each of these 3 VFSS metrics, which suggests these metrics may not be useful for detecting post-surgical dysphagia in this model.

In contrast, the group means for lick rate (i.e., tongue motility), pharyngeal transit time, and esophageal transit time were similar at baseline but different at the post-surgical time points, as shown in Fig. 6. ANOVAs based on change scores revealed statistically significant ($p \leq 0.05$) differences in lick rate and pharyngeal transit time, but not esophageal transit time, ($F_{3,34} = 4.470$, $p = 0.009$; $F_{3,34} = 3.956$, $p = 0.016$, respectively) at the acute recovery time point (Table 6). No significant differences in swallow function were evident at the chronic recovery time point (Table 7), indicating that acute changes in swallow function had returned to normal by 3 months post-surgery. Post hoc t tests were conducted only for the two significant acute recovery ANOVA change scores (i.e., lick rate and pharyngeal transit time). Results revealed that lick rate was significantly slower after unilateral RLN transection

compared to unilateral SLN transection ($diff_{\Delta uRLN-\Delta uSLN} = -0.522$; $p = 0.035$), bilateral SLN transection ($diff_{\Delta uRLN-\Delta bSLN} = -0.992$; $p = 0.011$), and sham surgery ($diff_{\Delta uRLN-\Delta sham} = -0.835$; $p = 0.047$), whereas pharyngeal transit time was significantly longer after bilateral SLN transection compared to unilateral SLN transection ($diff_{\Delta bSLN-\Delta uSLN} = 0.003$; $p = 0.009$). All other group comparisons for these two VFSS metrics were not statistically different ($p > 0.05$). Although not statistically different, esophageal transit time was noticeably longer for the unilateral RLN and bilateral SLN transection groups at the 1-week post-surgery time point (Table 8).

The final VFSS metric under investigation was PAS. At each time point, all mice in each of the four surgical groups had a score of 1 (i.e., no evidence of penetration or aspiration). Therefore, statistical analysis was not performed for this metric because there was no variability in the data (i.e., standard deviation = 0).

Model Refinement and Therapeutic Investigation: RLN Crush Injury and iVNS Treatment

Descriptive statistics for the two experimental groups (RLN crush without iVNS, and RLN crush with iVNS) are shown in Table 7. Initially, the four iVNS-treated mice were evenly split into 60-min ($n = 2$) versus 30-min ($n = 2$) treatment groups. However, the first mouse in the 60-min treatment group died intraoperatively due to respiratory distress, and the second mouse developed irregular breathing that was not resolved by lowering the stimulus intensity; therefore, treatment was prematurely ended at 50 min for this mouse. In contrast, the 30-min iVNS treatment duration was well tolerated by the other 2 mice, without adverse events. The 3 surviving iVNS-treated mice (one 50-min treatment and two 30-min treatment) were combined into a single iVNS treatment group for comparison with the control group ($n = 3$, RLN crush without iVNS treatment).

Post-surgery, all 6 mice underwent functional testing of VF mobility (i.e., laryngoscopy) once a week as planned until the study end point (3 months post-surgery). VFSS was not performed on these mice because results from the more severe RLN injury group (i.e., transection) revealed only a transient tongue motility deficit; no other significant swallow-related impairments were identified after RLN injury. Thus, we elected to defer this extremely labor intensive assay for a subsequent larger RLN crush/iVNS treatment study that will benefit from our VFSS analysis software that is currently under development.

VF Mobility—A total of 84 laryngoscopy videos (6 mice × 14 time points) were manually analyzed using a 3-point rating scale. As shown in Fig. 7, RLN crush injury caused immediate, ipsilateral VF immobility (i.e., VF mobility score = 0) in all 6 mice. Beginning at 2 weeks post-injury, iVNS-treated mice demonstrated markedly improved recovery of VF mobility compared to untreated mice. Although the small sample size precluded rigorous statistical analyses, an independent samples *t* test performed at only the final time point (12 weeks post-crush) revealed that treatment recovery after iVNS (mean = 1.67 ± 0.58, median = 2.00, $n = 3$) was significantly different compared to controls (mean = 0.34 ± 0.58, median = 0.00, $n = 3$), suggesting a beneficial treatment effect ($p = 0.047$).

Histological Results

Using our Sihler whole mount staining protocol, we were able to grossly map the laryngeal nerves (RLN and SLN) in this small mammal and show that the anatomic pattern is remarkably similar to humans (Fig. 8). This staining method also provided confirmatory evidence that the target laryngeal nerve was completely transected, without re-attachment throughout the post-surgical recovery period. Trans-illumination of Sihler stained specimens under our surgical microscope permitted identification of tiny RLN branches that were not visible during the surgical procedure. RLN branching was also apparent during post-mortem dissections, but only with extreme lateral retraction (Fig. 9). As lateral retraction of the RLN was avoided in our surgical approach, we expect that any existing RLN branches were likely included with the RLN trunk when it was isolated and transected. However, this hypothesis requires histological confirmation in our future studies.

Of the 20 combined specimens subjected to either Sihler staining or post-mortem dissection, most (80%) had 1–2 visible branches emanating from the main RLN trunk bilaterally (but not in a symmetrical pattern), in the vicinity of the 4th to 8th tracheal rings. A few specimens had RLN branching only on the right ($n = 2$) or left ($n = 1$) side, and one specimen did not have any visible RLN branches on either side. All branches disappeared as they approached the larynx, where they became too tiny to visualize using standard light microscopy methods.

A representative H&E stained transverse section of the murine larynx is shown in Fig. 10, which highlights important differences in VF structure and function between the mouse and human. However, striking cross-species similarity of the cartilaginous and muscular framework of the larynx is indeed apparent. For example, like humans, the murine thyroarytenoid muscle consists of medial and lateral bellies, as well as a more ventrally located oblique belly that has only recently been identified in humans [52].

Discussion

We successfully developed a mouse model of iatrogenic RLN injury with impaired VF mobility *and* swallowing function to serve as a translational platform for investigations of the pathological mechanisms contributing to poor functional outcomes and the development of novel regenerative treatment strategies. We used our “miniaturized” endoscopic [35] and fluoroscopic [32, 36] imaging assays to characterize VF mobility and swallow function, respectively, after transection injury. We included the SLN in our model development because of its hypothesized collateral innervation of intrinsic laryngeal muscles after RLN injury, which presumably contributes to VF synkinesis and resultant poor functional outcomes [2, 6, 7]. Thus, we investigated the effect of four distinct laryngeal nerve injury patterns: RLN transection (unilateral versus bilateral) and SLN transection (unilateral versus bilateral). We examined four clinically relevant time points for longitudinal assessment of functional outcomes: baseline (1 week prior to surgery), during surgery (immediately post-transection), an acute recovery stage (1 week post-surgery), and a chronic recovery stage (3 months post-surgery). A sham surgical group was included as a negative control. Additionally, we studied a potential therapeutic intervention (iVNS) in aged mice to better correspond to the average age of anterior neck surgical patients. Moreover, the recovery

period in our study roughly corresponds to over a decade in human years [53], thus providing additional translational perspective for human surgical patients with chronic adverse outcomes after iatrogenic RLN injury.

As hypothesized, unilateral RLN transection resulted in immediate, ipsilateral VF paralysis (i.e., immobilization in the paramedian position), suggesting the RLN motor innervation pattern of intrinsic laryngeal muscles in mice is similar to humans. As expected, bilateral RLN transection caused complete airway obstruction from the medialized, immobile vocal folds, resulting in intraoperative mortality. In contrast, SLN transection (unilateral or bilateral) had no visible effects on VF mobility. Importantly, our sham surgery group did not develop impaired VF mobility, thus validating the surgical technique itself had no confounding effects on functional outcomes.

Whereas unilateral RLN transection in mice resulted in chronic impairment of VF mobility, dysphagia was transient and limited to the *oral stage* of swallowing, specifically affecting lick rate (i.e., tongue motility). This finding is in alignment with a recent report of significant oral stage alterations (e.g., tongue shape and bolus formation) in *infant pigs* after unilateral RLN transection [54]; however, a related study showed no alteration in piglet suckling rate [20]. We suspect this difference may be because licking (drinking) behavior in adult mice requires marked tongue protrusion that visibly elevates the hyoid bone (and hence larynx), whereas suckling in piglets requires comparatively little movement of the tongue and hyoid. As the tongue is anatomically coupled to the larynx via the hyoid [55], the resultant VF immobility after unilateral RLN transection in mice may be causing an anchoring effect that hinders normal tongue protrusion during drinking. Alternatively, RLN injury in infant pigs was shown to affect EMG swallowing activity in muscles that are not directly innervated by the RLN, particularly the tongue [56]. In this case, muscle activity was decreased in lesioned animals prior to swallow initiation and during bolus transit, resulting in marked differences in tongue shape, movement, and timing, as well as corresponding differences in the size and shape of the bolus. These findings provide rationale for inclusion of EMG and other kinematic assessments of tongue function to further explore the link between RLN injury and altered lick rate in our model.

Moreover, these findings suggest that an RLN lesion may impact upstream neural connections between the numerous brainstem nuclei and/or cortical regions involved in swallowing [56]. In our study, we suspect the 4-day post-surgical VFSS time point provided an ample window for Wallerian degeneration, a stereotypical process that initiates degeneration of the myelin sheath and axons within 24–36 after nerve injury, paving the way for nerve regeneration [57]. Moreover, the act of surgically creating the nerve injury generates an immediate burst of action potentials that travel centrally along the injured axons to reach the neuronal cell bodies and their synaptic connections. This nerve injury signal triggers the necessary metabolic processes within the cell bodies to promote nerve regeneration and promote neural plasticity [58]. In the case of the RLN, the “injury signal” travels along the vagus nerve to stimulate the vagal ganglia (i.e., afferent/sensory neurons of the RLN) and the nucleus ambiguus in the brainstem medulla (i.e., efferent/motor neurons of the RLN), and their synaptic connections with the numerous brainstem and cortical regions involved in swallowing. Thus, our mouse model of RLN injury with resultant tongue

motility deficit at the 4-day post-surgical time point provides a suitable platform for systematic investigations of the peripheral and central effects of RLN injury and for exploring novel mechanisms to enhance neural plasticity and optimize functional outcomes.

Interestingly, esophageal transit time was noticeably (but not significantly) longer after RLN transection, resembling findings with infant pigs [20]. Given that esophageal dysphagia is a common report in humans after anterior neck surgical procedures [59, 60], we are currently strategizing alternative esophageal outcome measures via VFSS that may be more robust indicators of RLN injury for use in future experiments with this model. We also are exploring the possibility of performing EMG and manometry in this small animal for better detection and objective quantification of esophageal impairment.

In contrast to humans and other larger animal models of RLN injury, VF paralysis in mice does not result in aspiration during swallowing. As the sensory receptors of the RLN are located below the VFs and there is no aspirated fluid stimulating this region (based on our VFSS findings), the sensory component of the RLN is unlikely to contribute to the overall swallow pathology and recovery in our model. Instead, we suspect the dichotomy in recovery between VF mobility and swallowing function after RLN injury may be due to the mice adopting compensatory behavioral strategies during feeding to maintain adequate nutrition and hydration, as previously described for people [61–63].

This recovery dichotomy may also be due to technological limitations of our fluoroscope as well as species-related differences in the swallowing mechanism. For example, we have previously shown the pharyngeal stage of swallowing in mice is approximately ten times faster than humans [32, 36] Therefore, the 30 fps limitation of our fluoroscopy camera prevents sufficient temporal resolution to reliably quantify the numerous rapid events occurring during swallowing. Further, our low energy X-ray system prevents visualization of soft tissue and cartilaginous structures of the larynx and pharynx; therefore, quantification of swallowing function was largely limited to bolus flow dynamics. At no time was there evidence of laryngeal penetration or aspiration of the oral contrast agent, likely because mice are preferential nasal breathers whose larynx resides in the nasopharynx, inherently protected from the path of the bolus during swallowing [32, 36]. However, impaired VF mobility is a significant risk factor for penetration/aspiration in humans, thus highlighting the translational applicability of our mouse model.

Results for the SLN transection groups further support model development. We expected SLN transection would result in subtle, transient changes in VF mobility and swallowing function, which would be more pronounced after bilateral transection. However, VF mobility was unaffected by SLN transection, and dysphagia was evident only after bilateral SLN transection, which resolved by the 3-month post-surgery time point. Only the pharyngeal stage of swallowing was significantly affected by bilateral SLN transection, as evidenced by longer pharyngeal transit times. This finding is congruent with studies of infant pigs, in which SLN transection resulted in increased pharyngeal transit time, as well as increased bolus area and aspiration incidence [21, 22], with more severe outcomes for bilateral injuries [23].

Importantly, we refined our RLN transection (neurotmesis) model to include a more prevalent axonotmesis surgical injury type. We chose a crush injury because it is easier to standardize than experimental traction or thermal approaches. Additionally, because crush injury shows spontaneous recovery over time, treatments targeting accelerated recovery can be assessed. We tested this hypothesis by conducting a feasibility study of intraoperative vagal nerve stimulation (iVNS) as a novel regenerative strategy. In doing so, we expanded upon a recent study in young adult rats, whereby intraoperative *RLN stimulation* accelerated the recovery of VF mobility after RLN crush injury [29]. However, rather than stimulating the RLN, we chose the *cervical vagus nerve* as a more clinically relevant treatment site. Our rationale was based on the highly variable and extensive branching pattern of the RLN which renders it quite challenging, if not impossible, for surgeons to pinpoint the exact site(s) of injury [2, 64, 65]. Thus, iVNS may circumvent this problem by simultaneously targeting all RLN branches to promote widespread regeneration.

Although our study provides encouraging preliminary data that iVNS may improve recovery after RLN axonotmesis, larger studies must be conducted to establish optimal iVNS treatment parameters (e.g., stimulus frequency and intensity, treatment duration) and to characterize voice, respiratory, and swallowing outcomes in parallel with VF mobility. Furthermore, effects on RLN fiber types (motor, sensory, and autonomic/parasympathetic) must be considered, as each may require different stimulation parameters for optimal regeneration [43, 44, 66]. Nevertheless, the high clinical-translational potential of our proposed iVNS treatment strategy is supported by existing FDA-approved vagal nerve stimulation technology, for example continuous intraoperative nerve monitoring (CIONM) [67–69]. CIONM enables EMG monitoring of the VFs to detect RLN injury by providing periodic, low-level neuro-stimulation throughout the surgery via an electrode secured around the vagus nerve. Thus, if iVNS proves to be effective in promoting RLN regeneration, we propose the CIONM software could be modified to include settings appropriate for iVNS treatment, thereby expanding this technology from purely an RLN monitoring device into a robust therapeutic nerve regeneration strategy.

Additionally, we successfully performed laryngeal nerve mapping using post-mortem dissections and a Sihler whole mount staining technique. Results revealed multiple RLN branches terminating along the esophagus and larynx, similar to the variable innervation pattern described for the human RLN [70–73]. For this reason, our future studies will include histological confirmation in each mouse that all RLN branches at the injury site are effectively targeted, thus providing a methodological control to improve scientific rigor. We also performed basic histologic evaluation of the larynx using H&E staining of transverse sections, which confirmed the previously published, detailed description of the mouse larynx [33]. However, our ability to perform in vivo endoscopic assessment of the larynx for comparison with post-mortem histological assays provides a novel perspective of the similarities and differences between the mouse and human larynx. Given the extremely small size of mice, more in depth microscopic investigations (e.g., immunohistochemistry and transmission electron microscopy) will be essential for detailed laryngeal nerve mapping, as well as objective quantification of normal and pathological neuromuscular innervation and remodeling after laryngeal nerve injury and subsequent treatment interventions such as iVNS.

Other limitations of our study were that we did not investigate simultaneous injury of the RLN and SLN, we included a small sample size in our RLN crush/iVNS feasibility study, we did not include EMG recordings of the laryngeal muscles, nor did we include vocalization and respiratory assays for added translational impact. In addition, sex differences have not yet been explored in this model. Larger studies are underway to address each of these limitations.

A final notable limitation of our study involves interpretation of our endoscopic and fluoroscopic videos. For endoscopy, we used a qualitative Likert scoring system that introduces subjectivity, whereas, for fluoroscopy, we used a frame-by-frame manual analysis approach that is highly objective, but extremely labor intensive and therefore significantly slows the scientific discovery process. To overcome these limitations, we have developed custom software for semi-automated analysis of endoscopic [74] and fluoroscopic videos; validation studies are currently underway. We expect automation will permit high-throughput, objective quantification of the fast-paced breathing [35] and drinking [32, 36] behaviors observed in mice. Further, subtle changes in VF motion and swallowing function in mice that are difficult to detect with the human eye may be clinically relevant, as small changes in this small animal may in fact be large changes in humans. In addition, in human medicine, subjectivity is a known limitation of the “gold standard” endoscopic and fluoroscopic swallow tests, which results in poor inter- and intra-rater reliability [75–80]. Thus, we are in the process of adapting our software for validation with endoscopic and fluoroscopic videos obtained from humans, to further facilitate our translational research agenda.

In summary, we successfully developed a translational mouse model of iatrogenic RLN injury that demonstrates laryngeal (chronic) and swallowing (acute) dysfunction. We developed this model using our established endoscopic and fluoroscopic assays that permit longitudinal assessment in mice. We anticipate this new model will serve as a clinically relevant platform to (1) develop intraoperative strategies for RLN injury prevention, (2) elucidate the functional roles of the RLN versus SLN under normal versus lesioned conditions, (3) hasten our understanding of the molecular mechanisms contributing to poor functional outcomes after RLN injury, and (4) develop innovative regenerative treatment strategies to significantly accelerate and improve functional recovery of swallowing, voice, and breathing, which are all negatively impacted by RLN injury.

Acknowledgements

We graciously thank Dr. Christina Goldstein for providing translational surgical insight from an orthopedic perspective. Alex Hackworth and Connor (Beau) Burkett assisted with post-mortem laryngeal nerve dissections in mice. Marc Trautmann performed microtome sectioning of paraffin-embedded murine laryngeal specimens. We also acknowledge Roderic Schlotzhauer (MU Physics Machine Shop) for contribution to design and construction of the custom surgical table and laryngoscope tips essential to this study.

Funding

This study was partially funded by an NIH-T32 Grant (#2T32OD011126-38), which provided a postdoctoral stipend and research support for Megan Haney, DVM (sponsor: Lever).

References

1. Chandrasekhar SS, Randolph GW, Seidman MD, Rosenfeld RM, Angelos P, Barkmeier-Kraemer J, Benninger MS, Blumin JH, Dennis G, Hanks J, Haymart MR, Kloos RT, Seals B, Schreibstein JM, Thomas MA, Waddington C, Warren B, Robertson PJ, Surgery AAoO-HaN. Clinical practice guideline: improving voice outcomes after thyroid surgery. Otolaryngol Head Neck Surg. 2013;148(6 Suppl):S1–37. 10.1177/0194599813487301.
2. Mattsson P, Hydman J, Svensson M. Recovery of laryngeal function after intraoperative injury to the recurrent laryngeal nerve. Gland Surg. 2015;4(1):27–35. 10.3978/j.issn.2227-684X.2015.01.10. [PubMed: 25713777]
3. Brunner E, Friedrich G, Kiesler K, Chibidziura-Priesching J, Gugatschka M. Subjective breathing impairment in unilateral vocal fold paralysis. Folia Phoniatr Logop. 2011;63(3):142–6. 10.1159/000316320. [PubMed: 20938194]
4. Wang B, Yuan J, Chen X, Xu J, Li Y, Dong P. Functional regeneration of the transected recurrent laryngeal nerve using a collagen scaffold loaded with laminin and laminin-binding BDNF and GDNF. Sci Rep. 2016;6:32292. 10.1038/srep32292. [PubMed: 27558932]
5. Dionigi G, Wu CW, Kim HY, Rausei S, Boni L, Chiang FY. Severity of recurrent laryngeal nerve injuries in thyroid surgery. World J Surg. 2016;40(6):1373–81. 10.1007/s00268-016-3415-3. [PubMed: 26817650]
6. Crumley RL. Laryngeal synkinesis revisited. Ann Otol Rhinol Laryngol. 2000;109(4):365–71. 10.1177/000348940010900405. [PubMed: 10778890]
7. Hydman J, Mattsson P. Collateral reinnervation by the superior laryngeal nerve after recurrent laryngeal nerve injury. Muscle Nerve. 2008;38(4):1280–9. 10.1002/mus.21124. [PubMed: 18816603]
8. Crumley RL. Mechanisms of synkinesis. Laryngoscope. 1979;89(11):1847–54. 10.1288/00005537-197911000-00020. [PubMed: 502707]
9. Crumley RL. Unilateral recurrent laryngeal nerve paralysis. J Voice. 1994;8(1):79–83. [PubMed: 8167791]
10. Kovacic U, Sketelj J, Bajrović FF. Chapter 26: age-related differences in the reinnervation after peripheral nerve injury. Int Rev Neurobiol. 2009;87:465–82. 10.1016/s0074-7742(09)87026-8. [PubMed: 19682655]
11. Verdú E, Butí M, Navarro X. The effect of aging on efferent nerve fibers regeneration in mice. Brain Res. 1995;696(1–2):76–82. [PubMed: 8574688]
12. Tanaka K, Zhang QL, Webster HD. Myelinated fiber regeneration after sciatic nerve crush: morphometric observations in young adult and aging mice and the effects of macrophage suppression and conditioning lesions. Exp Neurol. 1992;118(1):53–61. [PubMed: 1397176]
13. Marawar S, Girardi FP, Sama AA, Ma Y, Gaber-Baylis LK, Besculides MC, Memtsoudis SG. National trends in anterior cervical fusion procedures. Spine. 2010;35(15):1454–9. 10.1097/brs.0b013e3181bef3cb. [PubMed: 20216341]
14. Howlader N, Noone A, Krapcho M, Miller D, Bishop K, Kosary C, Yu M, Ruh lJ, Tatalovich Z, Mariotto A, Lewis D, Chen H, Feuer E, Cronin K. SEER Cancer Statistics Review, 1975–2014. 2016. National Cancer Institute. Bethesda, MD. https://seer.cancer.gov/csr/1975_2014/. 2017.
15. Choi JS, Oh SH, An HY, Kim YM, Lee JH, Lim JY. Functional regeneration of recurrent laryngeal nerve injury during thyroid surgery using an asymmetrically porous nerve guide conduit in an animal model. Thyroid. 2014;24(1):52–9. 10.1089/thy.2013.0338. [PubMed: 24015805]
16. Kupfer RA, Old MO, Oh SS, Feldman EL, Hogikyan ND. Spontaneous laryngeal reinnervation following chronic recurrent laryngeal nerve injury. Laryngoscope. 2013;123(9):2216–27. 10.1002/lary.24049. [PubMed: 23817931]
17. Rosko AJ, Kupfer RA, Oh SS, Haring CT, Feldman EL, Hogikyan ND. Immunohistologic analysis of spontaneous recurrent laryngeal nerve reinnervation in a rat model. Laryngoscope. 2018;128(3):E117–22. 10.1002/lary.27004. [PubMed: 29226485]
18. Nishimoto K, Kumai Y, Yumoto E. Paradoxical movement of rat vocal folds following recurrent laryngeal nerve injury. Acta Otolaryngol. 2014;134(11):1164–71. 10.3109/00016489.2014.936625. [PubMed: 25315916]

19. Old MO, Oh SS, Feldman E, Hogikyan ND. Novel model to assess laryngeal function, innervation, and reinnervation. Ann Otol Rhinol Laryngol. 2011;120(5):331–8. 10.1177/000348941112000509. [PubMed: 21675590]
20. Gould FD, Lammers AR, Ohlemacher J, Ballester A, Fraley L, Gross A, German RZ. The physiologic impact of unilateral recurrent laryngeal nerve (RLN) lesion on infant oropharyngeal and esophageal performance. Dysphagia. 2015;30(6):714–22. 10.1007/s00455-015-9648-8. [PubMed: 26285799]
21. Ding P, Campbell-Malone R, Holman SD, Lukasik SL, Fukuhara T, Gierbolini-Norat EM, Thexton AJ, German RZ. Unilateral superior laryngeal nerve lesion in an animal model of dysphagia and its effect on sucking and swallowing. Dysphagia. 2013;28(3):404–12. 10.1007/s00455-013-9448-y. [PubMed: 23417250]
22. Ding P, Campbell-Malone R, Holman SD, Lukasik SL, Thexton AJ, German RZ. The effect of unilateral superior laryngeal nerve lesion on swallowing threshold volume. Laryngoscope. 2013;123(8):1942–7. 10.1002/lary.24051. [PubMed: 23670486]
23. Ding P, Fung GS, Lin M, Holman SD, German RZ. The effect of bilateral superior laryngeal nerve lesion on swallowing: a novel method to quantitate aspirated volume and pharyngeal threshold in videofluoroscopy. Dysphagia. 2015;30(1):47–56. 10.1007/s00455-014-9572-3. [PubMed: 25270532]
24. Lin YC, Dionigi G, Randolph GW, Lu IC, Chang PY, Tsai SY, Kim HY, Lee HY, Tufano RP, Sun H, Liu X, Chiang FY, Wu CW. Electrophysiologic monitoring correlates of recurrent laryngeal nerve heat thermal injury in a porcine model. Laryngoscope. 2015;125(8):E283–90. 10.1002/lary.25362. [PubMed: 26010439]
25. Kwak HY, Dionigi G, Kim D, Lee HY, Son GS, Lee JB, Bae JW, Kim HY. Thermal injury of the recurrent laryngeal nerve by THUNDERBEAT during thyroid surgery: findings from continuous intraoperative neuromonitoring in a porcine model. J Surg Res. 2015. 10.1016/j.jss.2015.06.066.
26. Paniello RC, Rich JT, Debnath NL. Laryngeal adductor function in experimental models of recurrent laryngeal nerve injury. Laryngoscope. 2015;125(2):E67–72. 10.1002/lary.24947. [PubMed: 25283381]
27. Woodson GE. Spontaneous laryngeal reinnervation after recurrent laryngeal or vagus nerve injury. Ann Otol Rhinol Laryngol. 2007;116(1):57–65. 10.1177/000348940711600110. [PubMed: 17305279]
28. Wang B, Yuan J, Xu J, Xie J, Wang G, Dong P. Neurotrophin expression and laryngeal muscle pathophysiology following recurrent laryngeal nerve transection. Mol Med Rep. 2016;13(2):1234–42. 10.3892/mmr.2015.4684. [PubMed: 26677138]
29. Monaco GN, Brown TJ, Burgette RC, Fargo KN, Akst LM, Jones KJ, Foecking EM. Electrical stimulation and testosterone enhance recovery from recurrent laryngeal nerve crush. Restor Neurol Neurosci. 2015;33(4):571–8. 10.3233/RNN-130334. [PubMed: 23902984]
30. Sharma N, Moeller CW, Marzo SJ, Jones KJ, Foecking EM. Combinatorial treatments enhance recovery following facial nerve crush. Laryngoscope. 2010;120(8):1523–30. 10.1002/lary.20997. [PubMed: 20641084]
31. Foecking EM, Fargo KN, Coughlin LM, Kim JT, Marzo SJ, Jones KJ. Single session of brief electrical stimulation immediately following crush injury enhances functional recovery of rat facial nerve. J Rehabil Res Dev. 2012;49(3):451–8. [PubMed: 22773203]
32. Lever TE, Braun SM, Brooks RT, Harris RA, Littrell LL, Neff RM, Hinkel CJ, Allen MJ, Ulsas MA. Adapting human videofluoroscopic swallow study methods to detect and characterize dysphagia in murine disease models. J Vis Exp. 2015;97:e52319. 10.3791/52319.
33. Thomas LB, Stemple JC, Andreatta RD, Andrade FH. Establishing a new animal model for the study of laryngeal biology and disease: an anatomic study of the mouse larynx. J Speech Lang Hear Res. 2009;52(3):802–11. 10.1044/1092-4388(2008/08-0087). [PubMed: 18806215]
34. Kingham PJ, Birchall MA, Burt R, Jones A, Terenghi G. Reinnervation of laryngeal muscles: a study of changes in myosin heavy chain expression. Muscle Nerve. 2005;32(6):761–6. 10.1002/mus.20409. [PubMed: 16007678]
35. Shock LA, Gallemore BC, Hinkel CJ, Szewczyk MM, Hopewell BL, Allen MJ, Thombs LA, Lever TE. Improving the utility of laryngeal adductor reflex testing: a translational tale of mice and men.

Otolaryngol Head Neck Surg. 2015;153(1):94–101. 10.1177/0194599815578103. [PubMed: 25832829]

36. Lever T, Brooks R, Thombs L, Littrell L, Harris R, Allen M, Kadosh M, Robbins K. Videofluoroscopic validation of a translational murine model of presbyphagia. Dysphagia. 2015;30(3):328–42. [PubMed: 25783697]
37. Björck G, Margolin G, Måbäck GM, Persson JK, Mattsson P, Hydman J. New animal model for assessment of functional laryngeal motor innervation. Ann Otol Rhinol Laryngol. 2012;121(10):695–9. 10.1177/000348941212101013. [PubMed: 23130547]
38. Paskhover B, Wadie M, Sasaki CT. Thyroarytenoid cross-innervation by the external branch of the superior laryngeal nerve in the porcine model. Laryngoscope. 2015;125(1):177–9. 10.1002/lary.24888. [PubMed: 25131261]
39. Lever TE, Simon E, Cox KT, Capra NF, O'Brien KF, Hough MS, Murashov AK. A mouse model of pharyngeal dysphagia in amyotrophic lateral sclerosis. Dysphagia. 2010;25(2):112–26. 10.1007/s00455-009-9232-1. [PubMed: 19495873]
40. Sang Q, Goyal RK. Swallowing reflex and brain stem neurons activated by superior laryngeal nerve stimulation in the mouse. Am J Physiol Gastrointest Liver Physiol. 2001;280(2):G191–200. [PubMed: 11208540]
41. Bridge PM, Ball DJ, Mackinnon SE, Nakao Y, Brandt K, Hunter DA, Hertl C. Nerve crush injuries—a model for axonotmesis. Exp Neurol. 1994;127(2):284–90. 10.1006/exnr.1994.1104. [PubMed: 8033968]
42. Hetzler LE, Sharma N, Tanzer L, Wurster RD, Leonetti J, Marzo SJ, Jones KJ, Foecking EM. Accelerating functional recovery after rat facial nerve injury: effects of gonadal steroids and electrical stimulation. Otolaryngol Head Neck Surg. 2008;139(1):62–7. 10.1016/j.otohns.2008.02.006. [PubMed: 18585563]
43. Al-Majed AA, Neumann CM, Brushart TM, Gordon T. Brief electrical stimulation promotes the speed and accuracy of motor axonal regeneration. J Neurosci. 2000;20(7):2602–8. [PubMed: 10729340]
44. Gordon T, Udina E, Verge VM, de Chaves EI. Brief electrical stimulation accelerates axon regeneration in the peripheral nervous system and promotes sensory axon regeneration in the central nervous system. Mot Control. 2009;13(4):412–41.
45. Hernández-Morato I, Valderrama-Canales FJ, Berdugo G, Arias G, McHanwell S, Sañudo J, Vázquez T, Pascual-Font A. Reorganization of laryngeal motoneurons after crush injury in the recurrent laryngeal nerve of the rat. J Anat. 2013;222(4):451–61. 10.1111/joa.12031. [PubMed: 23444899]
46. Rosenbek JC, Robbins JA, Roecker EB, Coyle JL, Wood JL. A penetration-aspiration scale. Dysphagia. 1996;11(2):93–8. [PubMed: 8721066]
47. Mu L, Sanders I. Sensory nerve supply of the human oro- and laryngopharynx: a preliminary study. Anat Rec. 2000;258(4):406–20. 10.1002/(sici)1097-0185(20000401)258:4<406:aid-ar9>3.0.co;2-5. [PubMed: 10737859]
48. Mu L, Sanders I. Sihler's whole mount nerve staining technique: a review. Biotech Histochem. 2010;85(1):19–42. 10.3109/10520290903048384. [PubMed: 19572223]
49. Su WF, Liu SC, Wang SD, Su WY, Ma KH, Huang TT. Nerve branches to the posterior cricoarytenoid muscle may complicate the laryngeal reinnervation procedure. Laryngoscope. 2015;125(2):419–23. 10.1002/lary.24944. [PubMed: 25267429]
50. Mu L, Sanders I. The human cricothyroid muscle: three muscle bellies and their innervation patterns. J Voice. 2009;23(1):21–8. 10.1016/j.jvoice.2007.08.001. [PubMed: 18191374]
51. Lever TE, Gorsek A, Cox KT, O'Brien KF, Capra NF, Hough MS, Murashov AK. An animal model of oral dysphagia in amyotrophic lateral sclerosis. Dysphagia. 2009;24(2):180–95. 10.1007/s00455-008-9190-z. [PubMed: 19107538]
52. Lee SH, Koh KS, Song WC. Oblique thyroarytenoid muscle in humans: an independent muscle or an accessory belly? Laryngoscope. 2018;128(7):1634–8. 10.1002/lary.27090. [PubMed: 29332305]
53. Dutta S, Sengupta P. Men and mice: relating their ages. Life Sci. 2015. 10.1016/j.lfs.2015.10.025.

54. Gould FDH, Yglesias B, Ohlemacher J, German RZ. Pre-pharyngeal swallow effects of recurrent laryngeal nerve lesion on bolus shape and airway protection in an infant pig model. Dysphagia. 2017;32(3):362–73. 10.1007/s00455-016-9762-2. [PubMed: 27873091]
55. Duffy JR. Motor speech disorders: substrates, differential diagnosis, and management. Amsterdam: Elsevier; 2005.
56. DeLozier KR, Gould FDH, Ohlemacher J, Thexton AJ, German RZ. Impact of recurrent laryngeal nerve lesion on oropharyngeal muscle activity and sensorimotor integration in an infant pig model. J Appl Physiol. 2018;125(1):159–66. 10.1152/japplphysiol.00963.2017. [PubMed: 29648522]
57. Gong L, Zhu Y, Xu X, Li H, Guo W, Zhao Q, Yao D. The effects of claudin 14 during early Wallerian degeneration after sciatic nerve injury. Neural Regen Res. 2014;9(24):2151–8. 10.4103/1673-5374.147946. [PubMed: 25657736]
58. Wu D, Murashov AK. Molecular mechanisms of peripheral nerve regeneration: emerging roles of microRNAs. Front Physiol. 2013;4:55. 10.3389/fphys.2013.00055. [PubMed: 23554595]
59. Scerrino G, Tudisca C, Bonventre S, Raspanti C, Picone D, Porrello C, Paladino NC, Vernuccio F, Cupido F, Cocorullo G, Lo Re G, Gulotta G. Swallowing disorders after thyroidectomy: what we know and where we are. A systematic review. Int J Surg. 2017;41(Suppl 1):S94–102. 10.1016/j.ijsu.2017.03.078. [PubMed: 28506421]
60. Shriver MF, Lewis DJ, Kshettry VR, Rosenbaum BP, Benzel EC, Mroz TE. Dysphagia rates after anterior cervical diskectomy and fusion: a systematic review and meta-analysis. Glob Spine J. 2017;7(1):95–103. 10.1055/s-0036-1583944.
61. Logemann JA, Larsen K. Oropharyngeal dysphagia: pathophysiology and diagnosis for the anniversary issue of diseases of the Esophagus. Dis Esophagus. 2012;25(4):299–304. 10.1111/j.1442-2050.2011.01210.x. [PubMed: 21595782]
62. Anderson KK, Arnold PM. Oropharyngeal Dysphagia after anterior cervical spine surgery: a review. Glob Spine J. 2013;3(4):273–86. 10.1055/s-0033-1354253.
63. Yue WM, Brodner W, Highland TR. Persistent swallowing and voice problems after anterior cervical discectomy and fusion with allograft and plating: a 5- to 11-year follow-up study. Eur Spine J. 2005;14(7):677–82. 10.1007/s00586-004-0849-3. [PubMed: 15692825]
64. Henry BM, Vikse J, Graves MJ, Sanna S, Sanna B, Tomaszewska IM, Tubbs RS, Tomaszewski KA. Extralaryngeal branching of the recurrent laryngeal nerve: a meta-analysis of 28,387 nerves. Langenbeck's Arch Surg. 2016;401(7):913–23. 10.1007/s00423-016-1455-7. [PubMed: 27251487]
65. Cetin F, Gurleyik E, Dogan S. Morphology and functional anatomy of the recurrent laryngeal nerve with extralaryngeal terminal bifurcation. Anat Res Int. 2016;2016:9503170. 10.1155/2016/9503170. [PubMed: 27493803]
66. Wong JN, Olson JL, Morhart MJ, Chan KM. Electrical stimulation enhances sensory recovery: a randomized controlled trial. Ann Neurol. 2015;77(6):996–1006. 10.1002/ana.24397. [PubMed: 25727139]
67. Schneider R, Randolph GW, Barczynski M, Dionigi G, Wu CW, Chiang FY, Machens A, Kamani D, Dralle H. Continuous intraoperative neural monitoring of the recurrent nerves in thyroid surgery: a quantum leap in technology. Gland Surg. 2016;5(6):607–16. 10.21037/gs.2016.11.10. [PubMed: 28149807]
68. Anuwong A, Lavazza M, Kim HY, Wu CW, Rausei S, Pappalardo V, Ferrari CC, Inversini D, Leotta A, Biondi A, Chiang FY, Dionigi G. Recurrent laryngeal nerve management in thyroid surgery: consequences of routine visualization, application of intermittent, standardized and continuous nerve monitoring. Updates Surg. 2016;68(4):331–41. 10.1007/s13304-016-0393-9. [PubMed: 27651334]
69. Deniwar A, Bhatia P, Kandil E. Electrophysiological neuromonitoring of the laryngeal nerves in thyroid and parathyroid surgery: a review. World J Exp Med. 2015;5(2):120–3. 10.5493/wjem.v5.i2.120. [PubMed: 25992326]
70. Barczyński M, Stopa M, Konturek A, Nowak W. The over-whelming majority but not all motor fibers of the bifid recurrent laryngeal nerve are located in the anterior extralaryngeal branch. World J Surg. 2016;40(3):629–35. 10.1007/s00268-015-3257-4. [PubMed: 26438241]

71. Miyauchi A, Masuoka H, Nakayama A, Higashiyama T. Innervation of the cricothyroid muscle by extralaryngeal branches of the recurrent laryngeal nerve. Laryngoscope. 2016;126(5):1157–62. 10.1002/lary.25691. [PubMed: 26509739]

72. Tang WJ, Sun SQ, Wang XL, Sun YX, Huang HX. An applied anatomical study on the recurrent laryngeal nerve and inferior thyroid artery. Surg Radiol Anat. 2012;34(4):325–32. 10.1007/s00276-011-0905-8. [PubMed: 22124577]

73. Chiang FY, Lu IC, Chen HC, Chen HY, Tsai CJ, Hsiao PJ, Lee KW, Wu CW. Anatomical variations of recurrent laryngeal nerve during thyroid surgery: how to identify and handle the variations with intraoperative neuromonitoring. Kaohsiung J Med Sci. 2010;26(11):575–83. 10.1016/S1607-551X(10)70089-9. [PubMed: 21126710]

74. Haney MM, Hamad A, Leary E, Bunyak F, Lever TE. Automated quantification of vocal fold motion in a recurrent laryngeal nerve injury mouse model. Laryngoscope. 2018. 10.1002/lary.27609.

75. Kelly AM, Leslie P, Beale T, Payten C, Drinnan MJ. Fibreoptic endoscopic evaluation of swallowing and videofluoroscopy: does examination type influence perception of pharyngeal residue severity? Clin Otolaryngol. 2006;31(5):425–32. 10.1111/j.1749-4486.2006.01292.x. [PubMed: 17014453]

76. Kelly AM, Drinnan MJ, Leslie P. Assessing penetration and aspiration: how do videofluoroscopy and fiberoptic endoscopic evaluation of swallowing compare? Laryngoscope. 2007;117(10):1723–7. 10.1097/MLG.0b013e318123ee6a. [PubMed: 17906496]

77. Scott A, Perry A, Bench J. A study of interrater reliability when using videofluoroscopy as an assessment of swallowing. Dysphagia. 1998;13(4):223–7. 10.1007/PL00009576. [PubMed: 9716754]

78. Kuhlemeier KV, Yates P, Palmer JB. Intra- and interrater variation in the evaluation of videofluorographic swallowing studies. Dysphagia. 1998;13(3):142–7. 10.1007/PL00009564. [PubMed: 9633153]

79. Lee JW, Randall DR, Evangelista LM, Kuhn MA, Belafsky PC. Subjective assessment of videofluoroscopic swallow studies. Otolaryngol Head Neck Surg. 2017;156(5):901–5. 10.1177/0194599817691276. [PubMed: 28195753]

80. Tohara H, Nakane A, Murata S, Mikushi S, Ouchi Y, Wakasugi Y, Takashima M, Chiba Y, Uematsu H. Inter- and intra-rater reliability in fibroptic endoscopic evaluation of swallowing. J Oral Rehabil. 2010;37(12):884–91. 10.1111/j.1365-2842.2010.02116.x. [PubMed: 20557434]

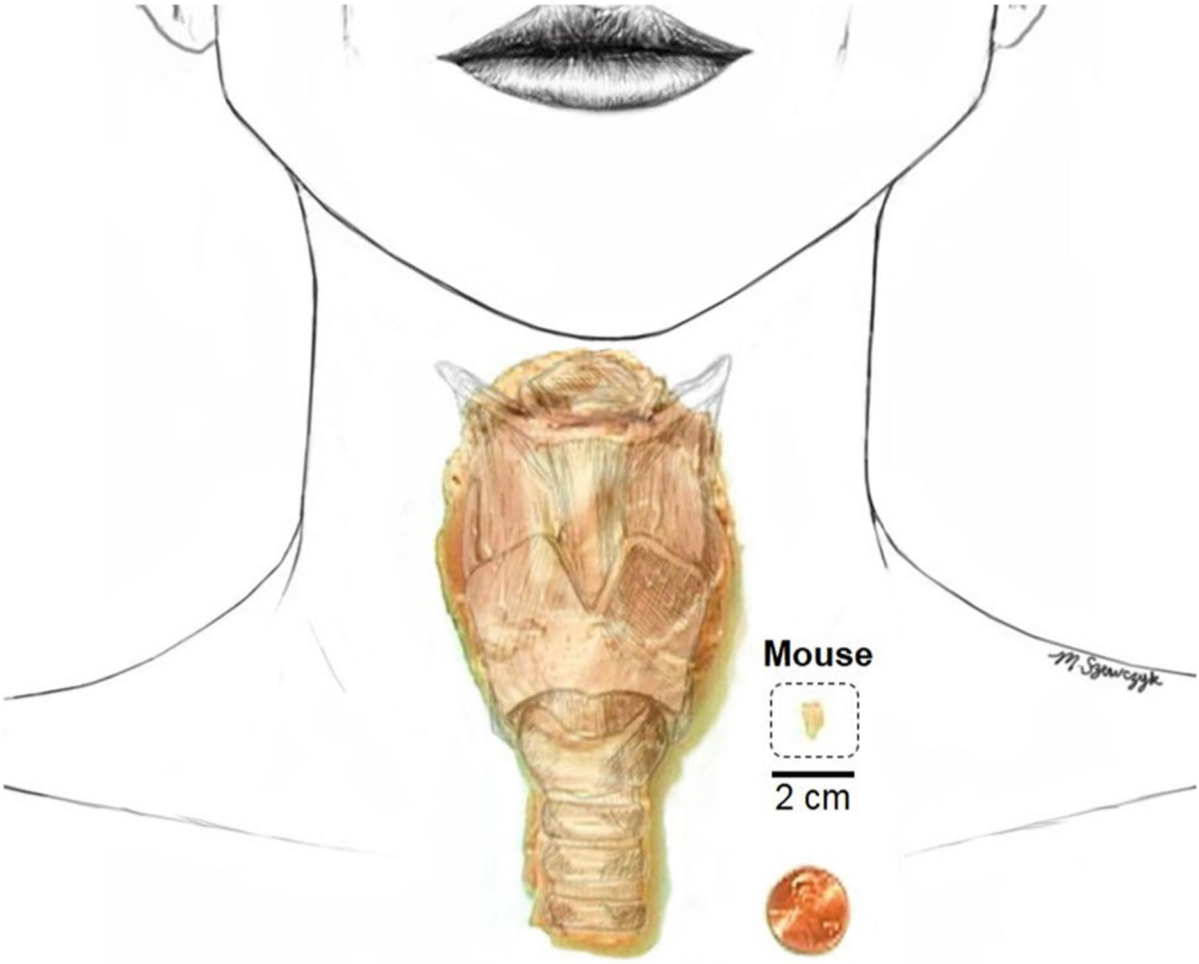

Fig. 1.

Size comparison between a human and mouse larynx. A photograph of side-by-side specimens of a human and mouse larynx next to a US penny (approximately 1.9 cm diameter), overlaid on a proportionately scaled schematic of a human head and neck. The cartilaginous/bony framework is drawn on both specimens for anatomical clarity. A 2-cm scale bar is shown for added size perspective

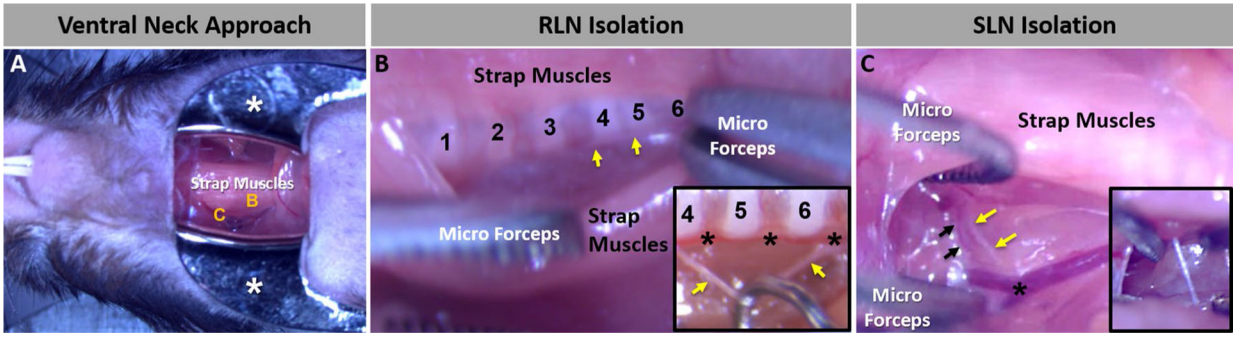

Fig. 2.

Microsurgical approach. **a** Our microsurgical approach in mice to access the laryngeal nerves via a midline ventral neck incision is typically a bloodless procedure. Micro-retractors (white asterisks) are used to maintain the large salivary glands out of the surgical field. The strap muscles obscure the RLN (**b**) and SLN (**c**), which are shown at higher magnification in images **b** and **c**, respectively. **b** To access the RLN, the strap muscles are carefully divided along the midline fascia and gently retracted with micro-forceps to expose the tracheal rings (numbered) and RLN (yellow arrows). The inset image shows a close-up of the target tracheal ring region, with the RLN (yellow arrows) isolated from the inferior thyroid artery (black asterisks) with a micro-hook in preparation for surgical transection. **c** To access the SLN, the strap muscles covering the lateral aspect of the larynx are gently elevated with micro-forceps to expose the SLN (yellow arrows) traveling alongside the superior laryngeal artery (black arrows) near the bifurcation of the common carotid artery (black asterisk). The inset image shows a close-up of the SLN (yellow arrow) isolated from the fascia with micro-forceps

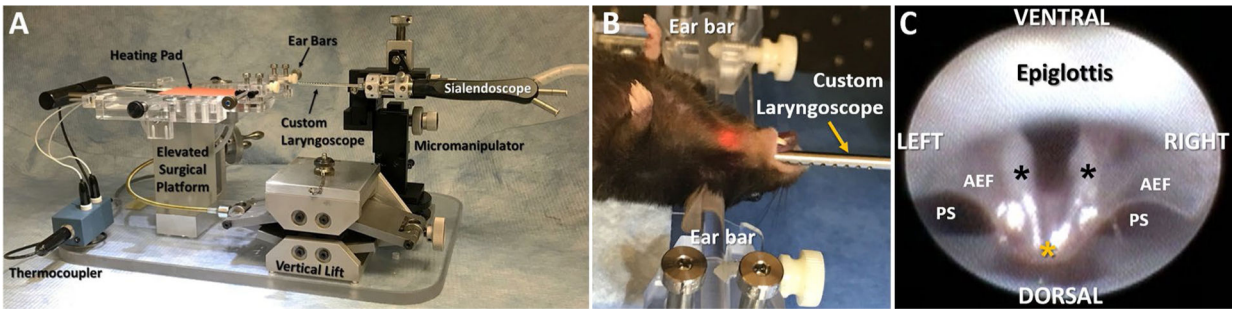

Fig. 3.

Laryngoscopy assay. **a** Lateral view of our custom endoscopy suite for mice, with labeled components. **b** An anesthetized mouse in dorsal recumbency undergoing laryngoscopy, with the head gently secured in ear bars. The micromanipulator in image **a** is used to precisely guide oral insertion, gentle advancement, and precise positioning of the sialendoscope (fitted with a custom laryngoscope) to visualize the larynx. **c** Representative endoscopic image of the murine larynx at maximum VF abduction during spontaneous breathing, taken from a 30 fps video at baseline (i.e., before surgery). Visible laryngeal structures of interest include the bilateral VFs (black asterisks), epiglottis, aryepiglottic folds (AEF), and pyriform sinuses (PS). In contrast to the human larynx, the VFs of mice retain midline proximity at the dorsal commissure (yellow asterisk), and the ventral commissure is consistently obscured by the epiglottis

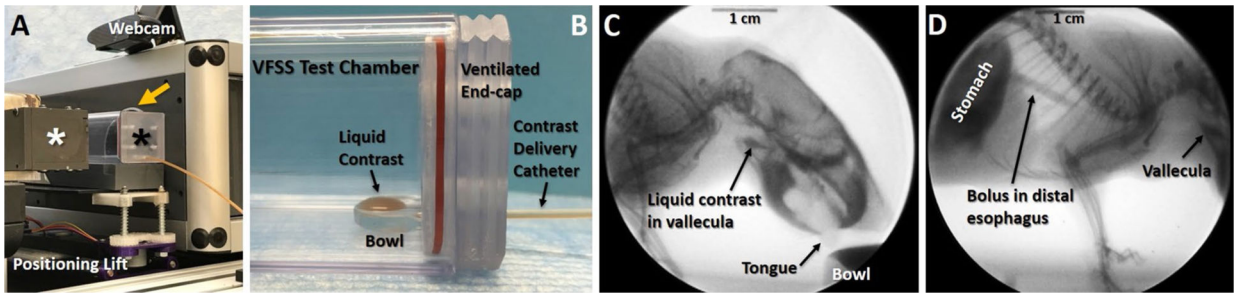

Fig. 4.

Videofluoroscopic swallow study (VFSS) assay. **a** A custom VFSS test chamber (black asterisk) is positioned in lateral view between the X-ray source (white asterisk) and image intensifier (yellow arrow) of our custom, miniaturized c-arm fluoroscope. The X-ray beam is turned on only when mice are actively drinking, identified via a webcam positioned above the test chamber. A remote-controlled positioning lift is used to readily maintain the mouse's aerodigestive tract within the fluoroscopy field of view. **b** Close-up of the VFSS test chamber in image **a**, designed to promote voluntary drinking of liquid contrast agent by mice with minimal behavioral distractions. Note the bowl within the test chamber is filled using a syringe delivery system that is manually controlled a few feet away from the fluoroscope. **c**, **d** Representative X-ray images from a 30 fps video of a mouse drinking in lateral view. Image **c** shows the oropharyngeal stage of swallowing, immediately prior to triggering of the swallow reflex. Note the liquid contrast agent accumulating in the vallecula within the pharynx, which is the stereotypical swallow trigger point in mice. Image **d** shows the esophageal stage of swallowing. Note the swallowed bolus traversing the distal esophagus into the stomach, while liquid contrast continues to accumulate in the vallecula prior to triggering a subsequent swallow

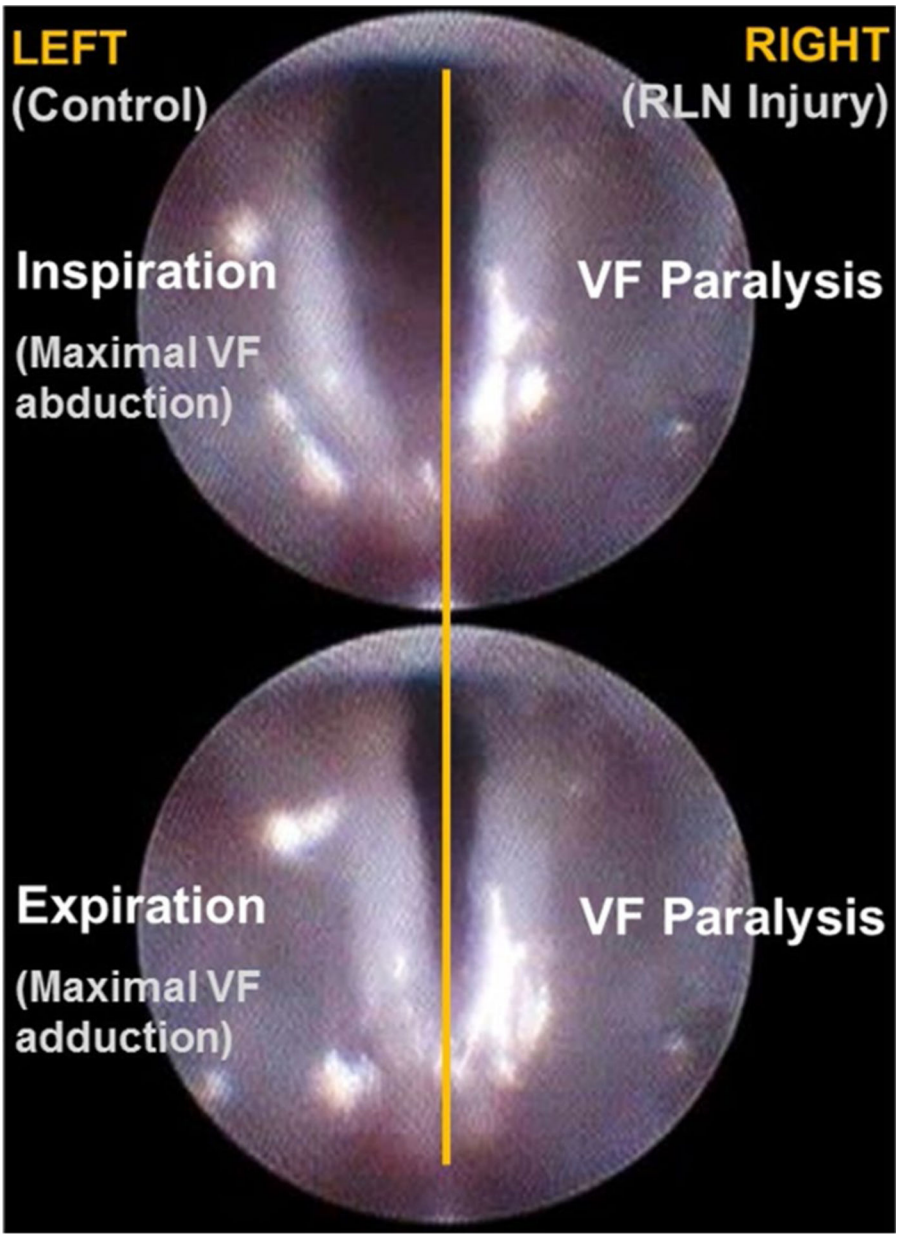

Fig. 5.

VF immobility after RLN transection. Endoscopic images showing the bilateral VFs of an anesthetized mouse during spontaneous breathing of room air after transection of the right RLN. *Top* Maximal VF abduction during inspiration. *Bottom* Maximal VF adduction during expiration. Note the paralyzed (immobile) right VF during the inspiratory and expiratory phases of the respiratory cycle

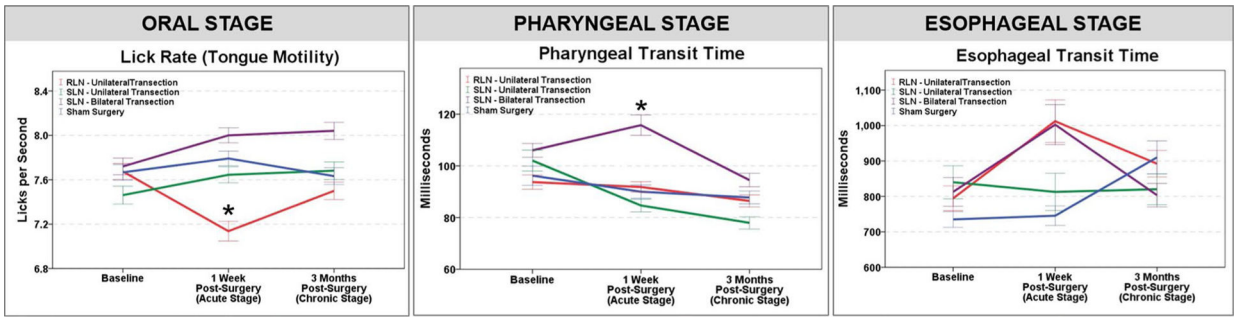

Fig. 6.

Effect of laryngeal nerve transection injury on swallow function. Of the four surgical groups investigated, only unilateral RLN transection and bilateral SLN transection had a statistically significant effect on swallow function. At the acute (1-week post-surgery) time point, lick rate (i.e., tongue motility) was significantly slower after unilateral RLN transection (red line, Oral Stage—left panel), and pharyngeal transit time was significantly longer after bilateral SLN transection (purple line, Pharyngeal Stage—middle panel). In addition, esophageal transit time was longer for the unilateral RLN and bilateral SLN transection groups (red and purple lines, respectively, Esophageal Stage—right panel); however, results did not reach statistical significance. At the chronic (3-month post-surgery) time point, swallow function was not significantly different from baseline function. Asterisk denotes statistical significance ($p < 0.05$) based on change scores; error bars = ± 1 SEM

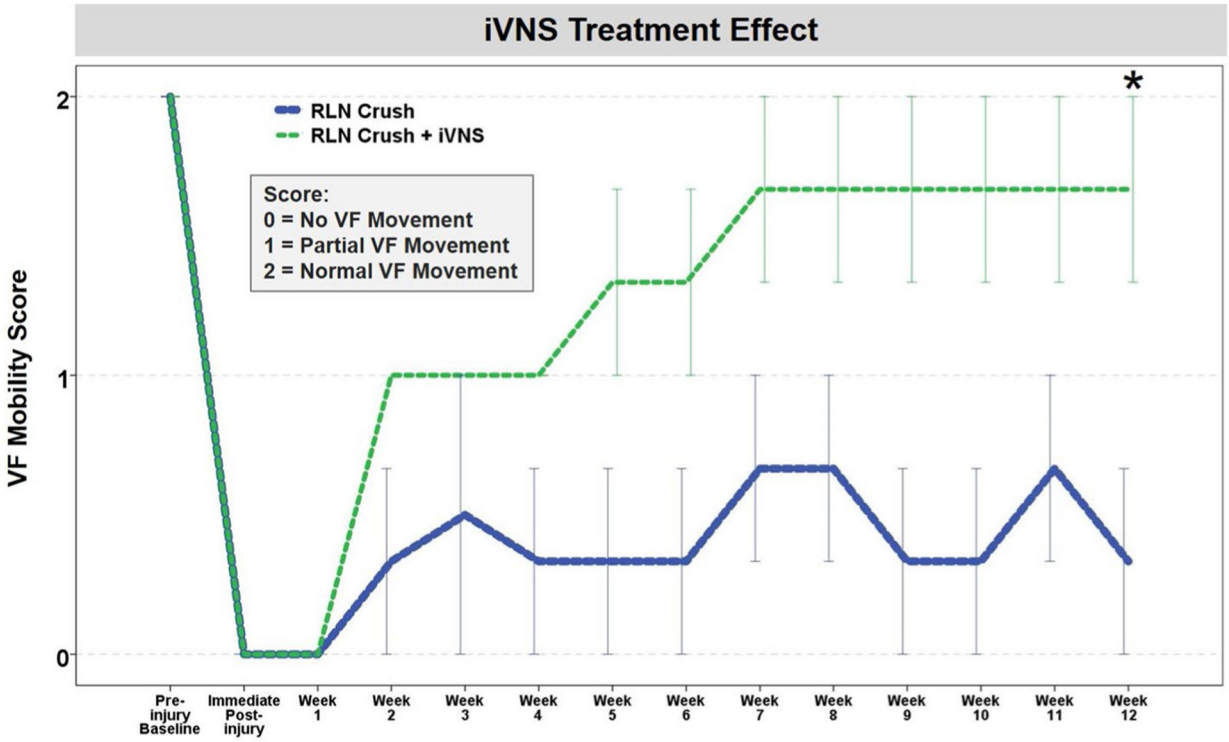

Fig. 7.

Effect of iVNS on VF mobility after RLN crush injury in aged mice. VF mobility improved in a stair step pattern after RLN crush injury in iVNS-treated mice > 1 year of age. Untreated age-matched mice fluctuated in VF mobility, with minimal improvement after a 12-week post-surgical recovery period. VF mobility was scored using a 3-point Likert scale. Error bars = ± 1 SEM; $n = 3$ mice per group. Time points with collapsed error bars indicate no within group variation of VF mobility scores. Asterisk = $p = 0.047$, based on a single t test at the final time point

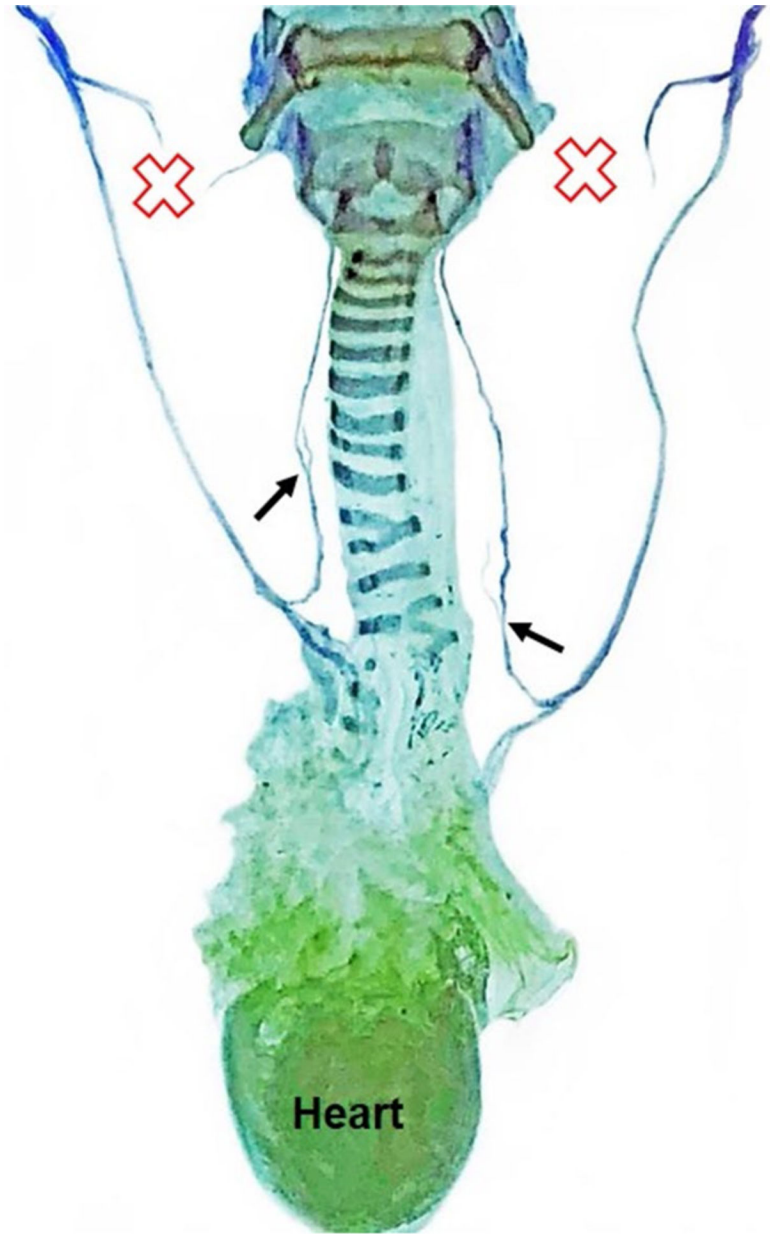

Fig. 8.

Sihler staining for laryngeal nerve mapping. A representative Sihler stained sample from a mouse in the bilateral SLN transection group demonstrates that the murine laryngeal framework and laryngeal nerve branching pattern are remarkably similar to humans. Red X indicates the location of SLN transection. Black arrows show the origin of nerve branches from the RLN trunk bilaterally. *CN X* Cranial nerve 10 (i.e., vagus nerve), *RLN* recurrent laryngeal nerve, *SLN* superior laryngeal nerve

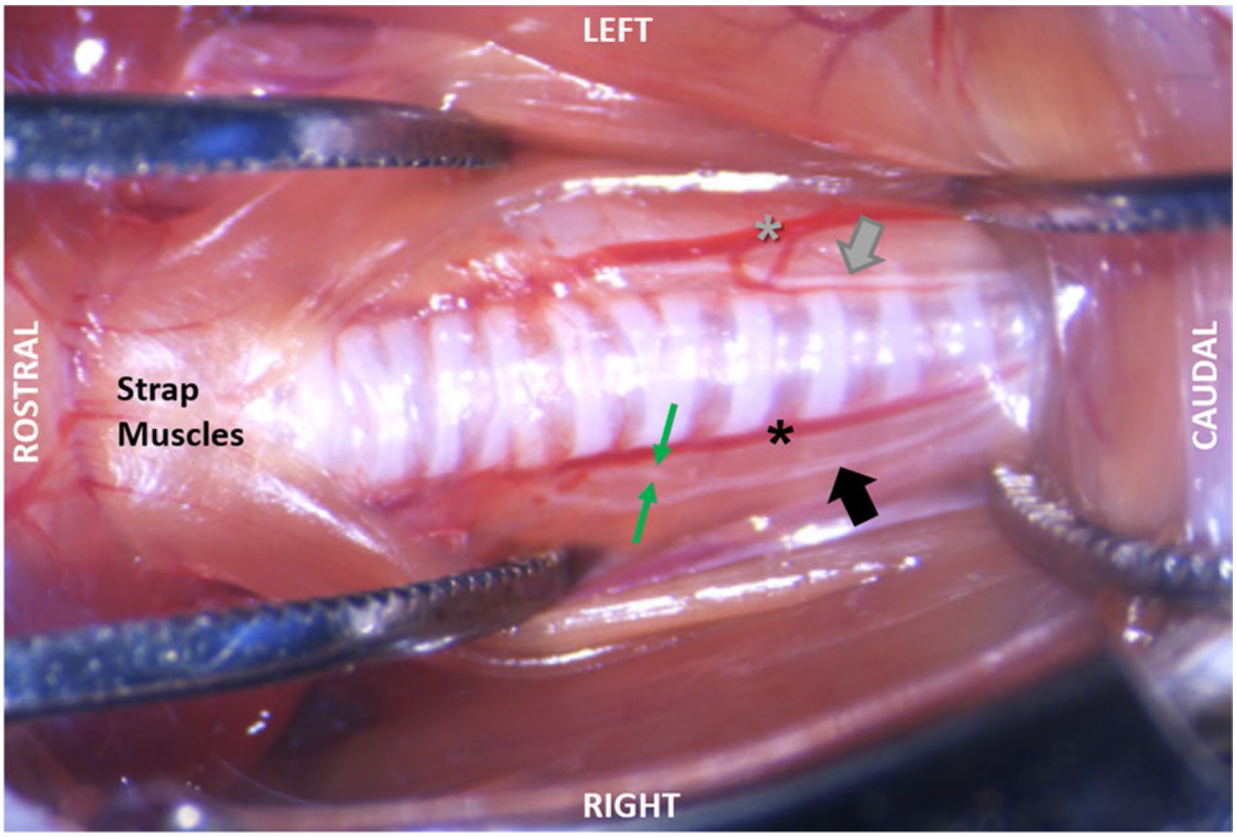

Fig. 9.

Post-mortem dissection demonstrating RLN branching. The left side shows that with minimal retraction of the soft tissues, as is used in our surgical approach, RLN branching is not visible. Instead, only the RLN trunk (gray arrow) can be seen running between the inferior thyroid artery (gray asterisk) and trachea. As shown on the right side, RLN branching is visible only during extreme lateral retraction of the midline strap muscles and fascia. In this specimen, the right RLN trunk (black arrow) has been pulled away from the inferior thyroid artery (black asterisk) to expose a single RLN branch (between the green arrows) near the 6th tracheal ring

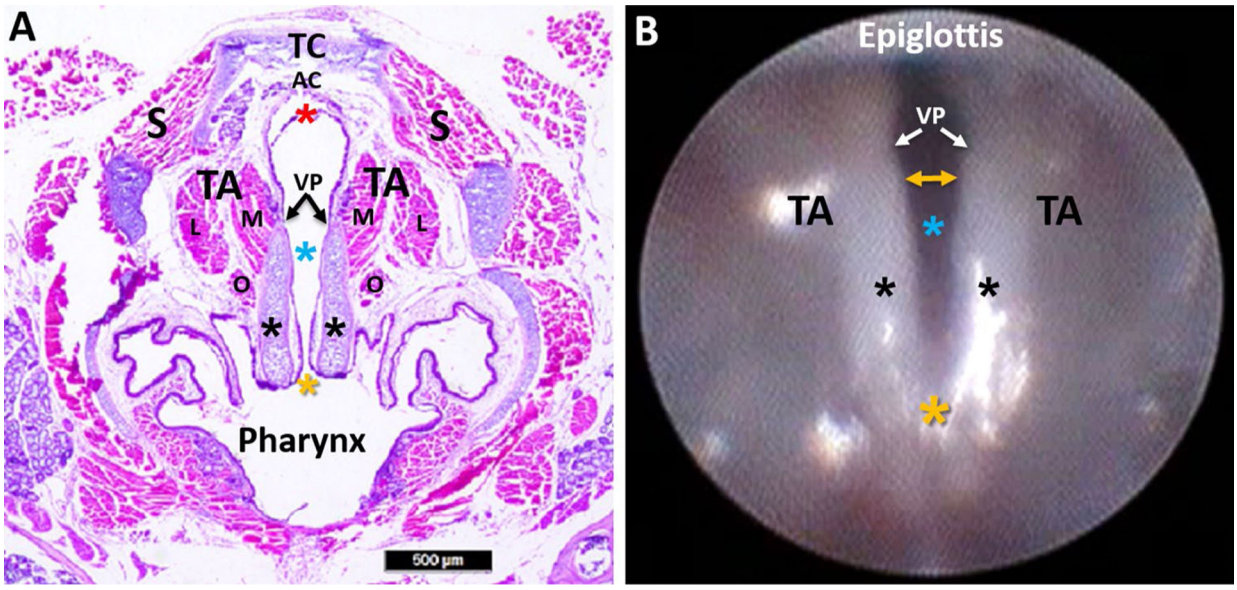

Fig. 10.

Murine laryngeal framework. **a** Hematoxylin and eosin (H&E) stained transverse Sect. (10 µm) of a mouse larynx at the level of the VFs, with labeled structures. **b** Endoscopic image of the murine VFs, with corresponding labeled structures from image **a.** In contrast to the human larynx, mice have proportionately larger arytenoid cartilages (black asterisks) and a proportionately smaller mucosal region extending beyond the vocal processes (VP) to the ventral commissure (red asterisk). In the mouse, the ventral commissure (which is obscured during laryngoscopy) is framed by a U-shaped alar cartilage (AC) that does not exist in humans. During spontaneous breathing in the mouse, the most dorsal portion of the arytenoids (yellow asterisk; dorsal commissure) remains relatively fixed near midline, serving as a pivot point for VF abduction and adduction. As a result, VF movement in the mouse is more readily apparent at the ventral (yellow bidirectional arrow in image **b** rather than the dorsal (posterior) region as in humans. *TC* thyroid cartilage, *AC* alar cartilage, *VP* vocal process, *TA* thyroarytenoid muscle (*M* medial belly, *L* lateral belly, *O* oblique belly), *S* strap muscles; blue asterisk: glottis; black asterisk: arytenoid cartilage; yellow asterisk: dorsal commissure; red asterisk: ventral commissure. Scale bar 500 µm

Table 1

VFSS metrics to detect and quantify dysphagia in mice

VFSS metrics	Operational definition
Lick rate	The number of licks per second (30 frames) during uninterrupted drinking. Each lick cycle begins with the jaw maximally opened and tongue protruding. Each subsequent maximal jaw excursion/tongue protrusion is counted as an individual lick cycle
Swallow rate	The number of swallows occurring during each 2-s (60 frames) episode of uninterrupted drinking. Each 2-s episode begins at the “rest frame” that immediately precedes triggering of the pharyngeal swallow (i.e., bolus flow from the valleculae to the esophagus)
Inter-swallow interval	The time (ms) between two successive, uninterrupted swallows during uninterrupted drinking. The start frame is the “rest frame” that immediately precedes triggering of the pharyngeal swallow. The end frame is the “rest frame” of the subsequent swallow. The number of frames between the two successive swallows is then divided by 30 frames per second (fps) to convert to time (ms)
Lick–swallow ratio	The number of licks during the inter-swallow interval (i.e., between two successive, uninterrupted swallows)
Pharyngeal transit time	The time (ms) it takes the bolus to be swallowed through the pharynx. The start frame is the “rest frame” that immediately precedes visible transfer of the bolus from the swallow trigger point (i.e., valleculae). The end frame is when the bolus tail enters the esophagus. The number of frames between the start and end frames is divided by 30 fps and converted to milliseconds (ms)
Esophageal transit time	The time (ms) it takes the bolus to be swallowed through the esophagus. The start frame is when the bolus tail enters the esophagus (i.e., the PTT end frame). The end frame is when the bolus tail enters the stomach. The number of frames between the start and end frames is divided by 30 fps and converted to milliseconds (ms)

Three to five measures of each VFSS metric are obtained for each mouse

Table 2

Sihler staining protocol for nerve mapping

Processing step	Duration	Target reaction
4% paraformaldehyde; change solution once a week	50–55 days	Tissue fixation
3% potassium hydroxide (KOH) with 3 drops of 3% v/v hydrogen peroxide per 100 mL; change solution twice a week	50–60 days	Maceration and depigmentation. *Endpoint* specimen becomes translucent and nerves can be clearly seen as white fibers under a transilluminated microscope
Sihler I solution; change solution twice a week	30 days	Decalcification
Sihler II solution; change solution every other week or more often if solution changes from dark blue to purple	30–40 days	Staining. *Endpoint* nerves become dark blue
Sihler I solution (with agitation); change solution 1–2 times as needed when it becomes blue or purple	24 h	Destaining. *Endpoint* nerves become dark purple but all other tissues become a transparent lavender color under a transilluminated microscope; check every 2–3 h
0.05% lithium carbonate (with agitation)	2 h	Neutralizing. *Endpoint* Nerves turn from purple to deep blue; check every 30 min under a transilluminated microscope
50% glycerine	4 days	Clearing. *Endpoint* when the finest nerve twigs can be seen clearly under a transilluminated microscope; check daily
100% glycerine with thymol crystals	n/a	Long-term preservation

Perform water washes between steps: rinse 5 times, incubate with agitation for 1 h, then rinse again 5 times

Table 3

Sample size, age, and body weight for surgical groups at the study start and end points

Surgical groups	Group sample size	Start of study				End of study			
		Males		Females		Males		Females	
		Age	Body weight	Age	Body weight	Age	Body weight	Age	Body weight
RLN transection (unilateral)	**9** (4M, 5F)	6.85 (0.45)	31.35 (2.09)	7.30 (0.00)	24.02 (0.53)	11.55 (0.45)	31.85 (2.68)	11.20 (0.12)	25.47 (0.69)
SLN transection (unilateral)	**9** (4M, 5F)	4.25 (0.03)	24.93 (1.03)	5.24 (0.27)	20.80 (0.77)	7.75 (0.03)	28.64 (0.89)	8.8 (0.29)	22.29 (0.64)
SLN transection (bilateral)	**10** (3M, 7F)	3.20 (0.16)	27.67 (2.07)	3.27 (0.09)	20.92 (0.39)	7.05 (0.42)	30.92 (0.97)	6.67 (0.08)	23.80 (0.70)
Sham surgery	**10** (6M, 4F)	3.87 (0.08)	26.33 (0.99)	4.00 (2.00)	22.92 (1.17)	7.62 (0.19)	31.58 (0.91)	7.60 (0.21)	25.11 (1.76)

Age months (standard error of the mean), *body weight* grams (standard error of the mean), *M* males, *F* females

Table 4

Change in VF mobility after surgical injury

Change score	Mean change score (standard deviation)			
	RLN transection (unilateral)	SLN transection		Sham surgery
		Unilateral	Bilateral	
1 week post-surgery minus baseline	− 2 (0)	0 (0)	0 (0)	0 (0)
3 months post-surgery minus baseline	− 2 (0)	0 (0)	0 (0)	0 (0)

Table 5

Descriptive statistic for VFSS metrics

VFSS metrics (units)	Baseline				1 week post-surgery				3 months post-surgery			
	Min	Max	$\bar{x}$	SD	Min	Max	$\bar{x}$	SD	Min	Max	$\bar{x}$	SD
RLN transection—unilateral												
Lick rate (# per second)	7.00	8.00	7.67	0.47	6.00	8.00	7.14	0.59	7.00	8.00	7.50	0.51
Swallow rate (# per 2 s)	2.00	6.00	3.70	0.86	2.00	6.00	3.66	0.75	2.00	6.00	3.74	0.96
Inter-swallow interval (ms)	0.23	1.30	0.65	0.21	0.27	1.03	0.64	0.17	0.37	1.30	0.62	0.24
Lick-swallow ratio (licks/swallow)	1.00	10.00	4.47	1.84	1.00	9.00	4.09	1.55	2.00	10.00	4.12	2.18
PTT (ms)	0.07	0.13	0.09	0.02	0.07	0.10	0.09	0.01	0.07	0.10	0.09	0.02
ETT (ms)	0.57	1.43	0.79	0.22	0.60	2.23	1.01	0.40	0.57	1.50	0.89	0.25
SLN transection—unilateral												
Lick rate (# per second)	7.00	8.00	7.46	0.51	7.00	8.00	7.64	0.48	7.00	9.00	7.68	0.52
Swallow rate (# per 2 s)	2.00	5.00	3.18	0.89	2.00	6.00	4.04	0.95	2.00	6.00	3.91	0.83
Inter-swallow interval (ms)	0.33	1.47	0.77	0.29	0.37	1.20	0.59	0.19	0.27	1.03	0.62	0.18
Lick-swallow ratio (licks/swallow)	2.00	10.00	5.51	2.37	2.00	9.00	3.96	1.60	1.00	7.00	4.16	1.51
PTT (ms)	0.07	0.17	0.10	0.03	0.07	0.13	0.08	0.02	0.03	0.10	0.08	0.02
ETT (ms)	0.53	1.50	0.84	0.30	0.53	2.23	0.81	0.35	0.60	2.07	0.82	0.29
SLN transection—bilateral												
Lick rate (# per second)	7.00	9.00	7.72	0.54	7.00	9.00	8.00	0.47	7.00	9.00	8.04	0.54
Swallow rate (# per 2 s)	3.00	8.00	4.92	1.05	3.00	7.00	4.26	0.92	2.00	6.00	4.06	1.04
Inter-swallow Interval (ms)	0.23	0.87	0.47	0.14	0.23	0.87	0.5513	0.13	0.33	1.20	0.59	0.17
Lick-swallow ratio (licks/swallow)	1.00	6.00	3.18	1.16	1.00	7.00	3.91	1.25	2.00	9.00	4.16	1.56
PTT (ms)	0.07	0.13	0.11	0.02	0.03	0.20	0.12	0.03	0.07	0.13	0.09	0.02
ETT (ms)	0.50	1.77	0.81	0.29	0.63	2.27	1.00	0.40	0.57	1.43	0.80	0.22
Sham surgery												
Lick rate (# per second)	7.00	8.00	7.67	0.48	7.00	9.00	7.79	0.46	7.00	9.00	7.63	0.53
Swallow rate (# per 2 s)	2.00	6.00	3.87	0.94	0.00	7.00	3.89	1.67	2.00	7.00	4.18	1.11
Inter-swallow interval (ms)	0.27	1.07	0.57	0.19	0.23	1.07	0.56	0.20	0.23	1.00	0.56	0.19
Lick-swallow ratio (licks/swallow)	1.00	8.00	3.93	1.63	0.00	8.00	3.35	1.95	1.00	7.00	3.55	1.61
PTT (ms)	0.07	0.17	0.10	0.03	0.07	0.13	0.09	0.02	0.07	0.13	0.09	0.02

VFSS metrics (units)	Baseline				1 week post-surgery				3 months post-surgery			
	Min	Max	$\bar{x}$	SD	Min	Max	$\bar{x}$	SD	Min	Max	$\bar{x}$	SD
ETT (ms)	0.53	1.40	0.74	0.16	0.53	1.40	0.75	0.19	0.43	1.70	0.91	0.33

PTT pharyngeal transit time, *ETT* esophageal transit time, *VFSS* metric values represent min (minimum), *max* (maximum), $\bar{x}$ (mean), and *SD* (standard deviation)

Table 6

Acute changes in swallow function

VFSS metrics (units)	Mean change score: 1 week post-surgery minus baseline (standard deviation)				*p* value ANOVA
	RLN transection (unilateral)	SLN Transection		Sham surgery	
		Unilateral	Bilateral		
Tongue motility (licks per second)	− 0.5 (0.6)	0.18 (0.5)	0.3 (0.5)	0.1 (0.5)	**0.009**
Pharyngeal transit time (ms)	− 2.0 (11.7)	− 1.7 (17.6)	8.9 (21.1)	− 5.1 (1.4)	**0.016**
Esophageal transit time (ms)	210.6 (273.2)	− 27.9 (318.3)	189.6 (248.7)	17.0 (106.9)	0.103

Bold *p* values indicate statistical significance

ms milliseconds

Table 7

Chronic changes in swallow function

VFSS metrics (units)	Mean change score: 3 months post-surgery minus baseline (standard deviation)				*p* value ANOVA
	RLN transection (unilateral)	SLN transection		Sham surgery	
		Unilateral	Bilateral		
Tongue motility (licks per second)	− 0.2 (0.5)	0.2 (0.4)	0.3 (0.5)	− 0.00 (0.6)	0.169
Pharyngeal transit time (ms)	− 7.5 (12.9)	− 23.8 (14.3)	− 11.0 (16.5)	− 7.7 (13.5)	0.066
Esophageal transit time (ms)	96.7 (128.5)	− 23.6 (248.2)	− 20.1 (177.2)	175.6 (224.8)	0.098

ms milliseconds

Table 8

Sample size and age range for experimental groups

Experimental group	Sample size			Age (months)
	Group	Sex		
		M	F	
RLN crush without iVNS (control; no treatment)	3	1	2	14.7 ± 2.3
RLN crush with iVNS (treatment)	3	1	2	13.3 ± 2.3

Age is expressed as mean ± standard deviation at the time of surgery *M* male, *F* female, *iVNS* intraoperative vagal nerve stimulation